Optimizing the Forces of Climbing Robots

by

Ausama H. Ahmed

M.Sc., Academy of Higher Education, Libya 2007
B.Sc., Altahadi University, Libya 2004

Thesis Submitted in Partial Fulfillment of the

Requirements for the Degree of

Doctor of Philosophy

in the

School of Engineering Science

Faculty of Applied Sciences

SIMON FRASER UNIVERSITY

Summer 2016

Approval

Name: **Ausama Ahmed**

Degree: **Doctor of Philosophy**

Title: ***Optimizing the Forces of Climbing Robots***

Examining Committee: **Chair:** Michael Sjoerdsma
Senior Lecturer

Carlo Menon
Senior Supervisor
Associate Professor

Edward Jung Wook Park
Supervisor
Professor

Flavio Firmani
Internal Examiner
Lecturer
School of Mechatronic Systems
Engineering

Alessandro Gasparetto
External Examiner
Professor
Department of Electrical, Management
and Mechanical
University of Udine

Date Defended/Approved: July 12, 2016

Abstract

Climbing robots have the potential to be used in diverse applications, such as cleaning sky scrapers, maintaining of maritime structures, and conducting search and rescues. The focus of this thesis is on optimizing the forces of a climbing robot loitering on vertical surfaces. The optimization is primarily achieved through on minimizing the maximum normal adhesion force on the tips of the legs of a six-legged climbing robot as well as the maximum torque experienced by the joints. In this theses, the model of a six legged robot is simplified into a two dimensional structure with three legs. Furthermore, this simplified robotic model was validated by the use of biomimicry; in which the stance of the ants is analyzed using the same model and verified that their posture indeed minimizes the maximum adhesion on the tips of their legs. The optimal normal adhesion force for a climbing robot is calculated using a closed form solution. For robots with position controlled legs, the effects of different geometrical parameters and the stiffness of the materials, used to build the structure of the robot are investigated with a focus on maximum normal adhesion. Calculation of the forces on the structure uses the Finite Element Method (FEM). For robots with force/torque controlled legs, the effect of geometric parameters, specifically the height and, the length of the robot and the position of the middle leg, are also investigated with emphasis on maximum normal adhesion. The effects of the investigated parameters are summarized and presented as guidelines for the design of climbing robots. Also, the non-linear and non-differentiable problem of minimizing the maximum torque on the joints of the robot, that uses the optimal normal adhesion force on the tips of their legs, is addressed only for robots with force/torque controlled legs. Finally, a transformation that converts the problem into a linear form is presented. The proposed method was found to outperform three other widely used algorithms in terms of speed and accuracy.

Keywords: Climbing robots; finite element method; biomimicry; normal adhesion optimization; maximum torque optimization

Dedication

With the love and respect the words cannot describe, I dedicate this thesis to my parents, grandmother, brothers and sisters and last but not least my wife. Without them, I wouldn't be where I am or who I am.

Acknowledgements

I would like to thank my senior supervisor, Dr. Carlo Menon for his support, counselling and encouragement throughout these last few years. His feedback and guidance helped me with the start and completion of this work. I would also like to thank Dr. Ed Park and Dr. Bill Gruver for their valuable feedback. I am equally grateful to Dr. Flavio Firmani and Dr. Alessandro Gasparetto for agreeing to be examiners.

Special thanks to everyone in MENRVA group for their help, advices, support and friendship, especially Juan Pablo, Yasong Li, and Ahmed.

Big thank goes to my parents, and siblings for their support every step of the way, to my wife and Sama and Sana for their patient and support, and to my friends, specially Ali, Ali and Sultan, whose support helped me to realize this accomplishment.

Table of Contents

List of Tables

List of Figures

List of Acronyms

FEM	Finite Element Method
CoM	Center of Mass

Chapter 1.

Motivation and Objectives

1.1. Motivation

Climbing robots mainly are designed to be used in situations where the availability of humans is risky and expensive, either it is unsafe for a human worker or it requires a huge amount of work/tools for the human to access and succeed at the task. Robots could be used in inspection and cleaning of dangerous and hard to reach places such as pipes, wind turbine blades and high-rises, in hazardous environments such as nuclear plants and space, and in security and military applications. There are over 600,000 bridges in the US alone, and more than 10,000 skyscrapers measuring at least 100m high world wide [1], around 225,000 turbines spinning worldwide as of 2012 [2], and 437 operational civil nuclear power reactors in the world [3], and these are only some of the structures where climbing robots could be used at.

Climbing robots have different designs such as, legged, tank and wheel-legged. The success of the climbing process highly depends on the performance of the attaching mechanism which should be able to withstand the pulling forces required to keep the robot on the wall. The different mechanisms utilized by the climbing robots include dry/wet adhesion, suction, magnetism and spines or claws. Legged robots have the potential to be more dexterous than other designs, because it can traverse complex environments.

A wall climbing robot is not only required to be light, but also to carry a large payload typically comprised of the necessary equipment to accomplish the required tasks. This thesis investigates increasing the payload by minimizing the maximum normal force, on the tips of the legs, required to adhere to the wall. Increasing the

payload is investigated for the case of using position controlled motors and the case of using torque controlled motors. Minimizing the maximum torque on the joints can also increase the life of the motors. Using low torque, and therefore current, decreases the heat generated in the motors, which in turn increases the life time of the motors.

1.2. Objectives

The overarching goal of this thesis is to minimize the forces on the structure of climbing robots, specifically, normal forces on the feet of the robot and the torques on the joints. Such a goal is divided into the following objectives:

Objective 1: Minimizing the normal adhesion force on the tips of the legs of climbing robot.

Objective 2: Designing the structure of the robots, with either position-controlled legs or force/torque controlled legs, to optimize the normal adhesion force required to climb vertical surfaces.

Objective 3: Minimizing the maximum torque on the joints of the climbing robot, with force/torque controlled legs, without compromising the optimal normal adhesion force requirement on the tips of the legs.

1.3. Thesis Layout

Chapter two is a literature review. The first objective is presented in Chapter three. The second objective is extended amongst Chapters four and five; Chapter six is used to verify the modelling and the simplifications used in the previous chapters. While the last objective is studied in Chapter seven.

Chapter 2.

Literature Review

A review of climbing robots and the techniques used to optimize their climbing abilities on flat surfaces is briefly presented in this first section. The control type of the motors used in robots, either by position or torque, is listed also in the first section. To the best of the author's knowledge, no minimization for the maximum torque of a climbing robot has so far been presented in literature. This problem of minimizing the maximum torque could be solved using different optimization techniques, which are reviewed in the second sub-section of this chapter. Variable stiffness materials, which are used in Chapter 4 to minimize the maximum normal adhesion are presented last.

2.1. Climbing Robots

Legged climbing robots can potentially be more versatile than those using other mechanisms such as wheels, frames, and treads, because they have the potential to handle a wide variety of terrains. Legged robots vary in the number of legs used to climb; ranging from; two to six, and higher, with or without the use of a tail.

Climbing robots use different mechanisms to adhere to surfaces such as magnets, negative pressure, grippers, spines/claws, and electrostatics. The effect of different adhesion mechanisms on the climbing surface's materials, the roughness of the surface, and the power consumption are listed in Table 2.1. The scope of the thesis focuses on the adhesions that are mounted on the tips of the legs of the robots.

Table 2.1. Different attachment types

	Materials	Rough/Smooth Surfaces	Power Consumption	Note
Magnets [4]–[6]	Only limited to ferrous surfaces	Any	Low	
negative pressure [7]–[9]	Any	Only smooth	High	
Vortex [10]	Any	Any	High	
Spines/Claws [11]–[14][15]	Any	Only rough	Low	Ultrasonic/Sonic Driller/Corer consumes high power, because it uses ultrasound to dig into rocks.
Electrostatic [16], [17]	Any	Any	High	Requires large area of contact
Bio mimetic [18]–[23]	Any	Only smooth	Low	
Chemicals [24]–[28]	Any	Any	Low	Consumes materials as it is used, fails if not enough is used.
Grippers	Any, see notes	Any, see notes	Low	The ability to traverse materials and surfaces depend on the adhesion type used on the gripper.

Most two-legged robots use magnets, suction and grippers. four and six legged robots use all the mechanisms listed in Table 2.1, except the Vortex and the active electrostatic. Active electrostatic is not being used in the legged climbing robots because it requires a large area of contact with the surface, which makes it more suitable for tank type robots. Vortex adhesions are not used with legged climbing robots so far, although vortex adhesion should be an applicable method to use for climbing.

Magnets have the problem of working only on ferrous surfaces, and are currently being used in robots that inspect and maintain large tanker ships. Spines/Claws are used to climb either rough surfaces such as bricks or soft materials such as textile fabric. The biomimetic adhesives utilize the Van Der Waals effect, observable in the way that geckos adhere to surfaces. Robots that utilize chemicals use materials such as duct tape [22] or hot glue [28] to stick to the surface.

A survey of the motors' control for the climbing robots in the literature is listed in Table 2.2. The most used control type, listed in 17 out of 22 robots, is the position control. Robug III uses force control but not many details are available about the type of sensors it uses.

Table 2.2. Climbing robots and the type of motors used.

Robot	Force control	Motor type	Sensors
REST [29]	N/A	Servo motors	Encoder, proximity, and current sensors
Stickybot [30] [31]	Yes	Servo motors	Hall effect sensors
Stickybot III [32]	Yes	Servo motors	Hall effect sensors
Spinybot II [14]	No	Servo motors	No
RiSE V2 [33]	Yes	DC motors	Stress, hall effect, current, and force sensors
Robug III [34]	Yes	Pneumatic actuators	N/A
Climbing the walls [35]	No	DC motors	Touch sensors
Robot by [24]	No	DC motors	No
Robot by [36]	No	Servo motors	Touch, and+ infrared sensors
Robot by [35]	No	Servo motors	Touch sensors
ROMA[37]	No	1 Servo motor,+ 8 AC motors	No
Robot by [38]	No	Servo motors	No
3Dclimber [39]	No	3 DC motors + 3 AC motors	FSR sensors
Treebot [40]	No	Linear motors	No
RiSE V3 [41]	Yes	DC motors	Stress, hall effect, current, and force sensors, Force sensitive link
Robot by [42]	No	Fluid actuators	No
4Steel robot [43]	No	4 Servo motors + 4 linear motors	Contact, and infrared sensors
Lemur II [44]	No	DC motors	No
CLIBO [45]	No	Servos motors	Torque sensors

Abigaille III [19]	No	DC motors	Potentiometers, and infrared sensors
CLASH [46]	No	DC motors	No
ASTERISK [47]	No	Servo motors	Force sensors

Many robots in Table 2.2 utilize force sensors, but not all of the robots use them to gain force control. Robots indicated by [35] and [36] use touch sensors to make firm contact with the surface, while the 4Steel robot uses touch sensors to activate the suction mechanism when it comes into contact with the surface. CLIBO uses the built in torque measurements from the servos to check whether or not the leg is gripping to the climbing surface.. The only robots that use force to distribute the load between the legs are the RiSE and the Stickybot robots. RiSE uses force control to distribute the shear force among the legs, and to assure the legs remain in contact with the surface after moving from the previous position. Stickybot also uses force sensors to distribute the shear force amongst the legs of the robot.

The design of some climbing robots was inspired by nature's living organisms, including geckos [20], spiders [18], cockroaches [12] or a combination of different species, such as geckos and cockroaches [33]. The arrangement and inclination of the legs are not the same among different robot designs. In fact, some of the robots, including Spinybot II [14], have their legs incline forward, while others, including Abigaille III [19], have some legs incline forward and others backward. Some robots, including the RiSE and Digbot [12], [48], have their legs on the sides of their bodies, while still others, including Abigaille II [18], have legs symmetrically distributed around their bodies.

Insects as well as robots use different gaits to move and traverse obstacles. Most climbing robots either use a two-step gait or a gait that moves one leg at a time. Two-step gaits are used mainly for a fast walk/run, as they require the minimum number of transitions for a single step. In contrast, moving one leg at a time requires the maximum number of legs to be in contact with the climbing surface at a time, which provides higher forces for the robot to adhere to the climbing surface.

Most of the force analysis on the robot's body is investigated using the quasi-static method [4], [18], [19], [21]–[23], [49], [50] instead of the Finite Element Method (FEM) [51]. FEM is able to provide more accurate results as it takes into account the flexibility and the shape of the analyzed structure. The results provided by FEM have unit-less dimensions and could be scaled to fit bigger and smaller structures as long as the second moment of area is fixed. A survey about the optimization algorithms that could be used to minimize the maximum torque for a force control robot is presented in the next section.

2.2. Optimization

Optimization has been applied to a wide variety of different industrial applications, including computing [52]–[54], communication [54], [55], manufacturing [56], and robotics and control [57], [58]. In robotics, optimization has been used in different aspects such as optimizing the gait cycle of walking [59]–[61] and climbing robots [47], motion [62], [63] path planning [64], and navigation [65].

Optimizing a problem with one objective could be solved using different types of algorithms, such as Probabilistic and Iterative algorithms. Probabilistic algorithms are particularly suitable when no information about the initial conditions are provided; Genetic algorithms [66], [67], Simulated Annealing and Ant Colony algorithm [68] are the most widely used probabilistic algorithms. However, they seek a near optimal solution and may require a long time to converge to a solution within a desired accuracy [69]. Iterative search techniques, such as the Nelder-Mead algorithm and the Interior-Point Method[52], [53], [70], can provide a solution within an accuracy specified by the user, which generally provides local solutions. While methods that combine probabilistic and iterative search techniques have been explored, their complexity is inevitably very high [68], [69], [71].

2.3. Variable stiffness materials

The reliability of climbing robots depends on many aspects; one important aspect is the efficiency of the adhesion used to keep the robot on the vertical climbing surface. The stronger the adhesion on the tips of the legs is, the more reliable the climbing process is. In this chapter, the maximum required adhesion force on the tips of the legs is minimized by using stiffness changing smart materials [72]–[76]. The adhesion could be optimized by altering the geometry of the robot, which could be done in the initial design stage of the robot; however, for a fixed structure, the adhesion could be optimized by changing the stiffness of the legs. The stiffness of the legs of the robot could be altered using stiffness changing smart materials. These are being applied in different fields, such as aerospace applications to morph airplane wings [77] and as a bandage to treat lower extremity disorder [78]. Changing the elasticity of the smart materials could be done using different techniques, such as capacitive shunting [73], shape memory alloy [74] and shape memory polymers [75], [76]. Changing the stiffness of the smart materials is accomplished using electrical, thermal, chemical or magnetic stimulus [72].

Chapter 3.

Optimal Adhesion for Legged Robots

3.1. Introduction

In this chapter, the problem of how to minimize the maximum adhesion of climbing robots loitering on vertical surfaces is addressed. The solution of the specific problem is desirable, as it minimizes the amount of force required on the individual feet of the robot. The optimal solution for the problem allows the climbing robot to climb using weak adhesion attachments yet successfully walk on vertical surfaces. Using weaker adhesion also allows the use of motors that are weaker than those required if the maximum adhesion on the tips of the legs is not minimized.

3.2. Robotic Model

The six legged robot considered here is simplified into a two-dimensional, three legged robotic structure, see Figure 3.1-a. The free body diagram of the robot is shown in Figure 3.1-b; the model only takes into account the position of the center of mass and the tips of the legs.

In a static case, the following equilibrium of the forces must be met

$$\sum F_X = f_{xf} + f_{xm} + f_{xh} - mg = 0 \quad (3.1)$$

$$\sum F_Y = f_{yf} + f_{ym} + f_{yh} = 0 \quad (3.2)$$

$$\sum M_Z = h \cdot mg + L_f \cdot f_{ym} + L_T \cdot f_{yf} = 0 \quad (3.3)$$

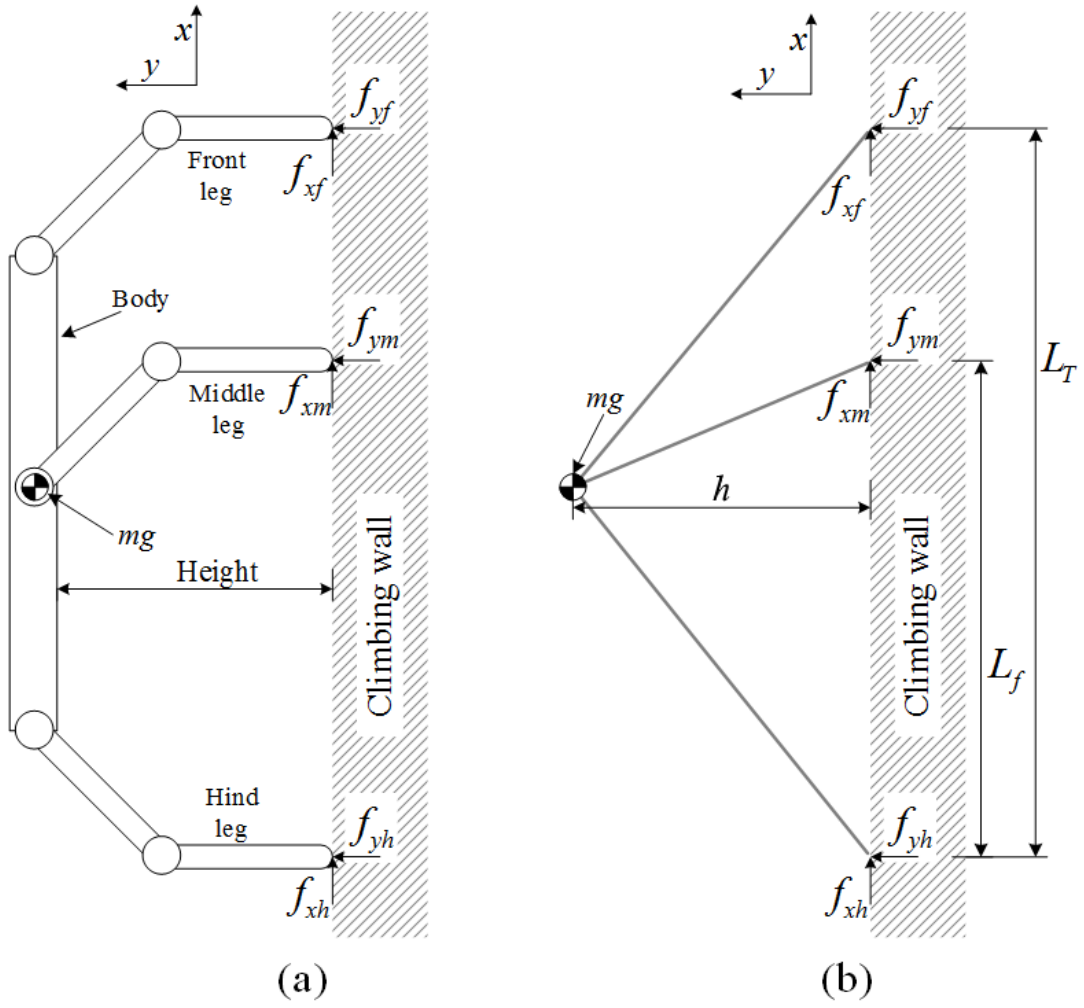

Figure 3.1. (a) Shows the robotic model, (b) Shows the simplified model

where F_X, F_Y are the forces acting along the considered x-axis, y-axis respectively. M_Z is the z-axis moment around the hind leg. f_{xf}, f_{xm} and f_{xh} are the shear forces and f_{yf}, f_{ym} and f_{yh} are the normal forces on the tips of the front, middle and hind legs respectively, mg is the weight of the robot at the center of mass CoM, h is the height of the robot, L_f is the distance between the hind and the middle legs and L_T is the distance between the front and the hind legs.

3.3. Minimizing the Maximum Adhesion

The fitness function $\Psi(x)$ for minimizing the maximum adhesion of the robotic model, given in Figure 3.1, is chosen to be as follows:

$$\Psi(x) = \min_{f_{xi}, f_{yi}} \big(\phi(f)\big), \quad \text{where } i = f, m, h \tag{3.4}$$

$$\phi(f) = \max\big(f_{yf}, f_{ym}, f_{yh}\big) \tag{3.5}$$

The optimal solution for the problem is the set of forces on the tips of the legs that minimizes the maximum adhesion force. The problem could be solved using traditional optimization techniques such as the Newton method, gradient descent and GA. In fact, [79] used GA to solve the problem, in which the authors minimized the maximum normal force while using Equations (3.1) to (3.3) as constraints. However, a closed form solution could be derived. Equation (3.3), could be rewritten as follows:

$$h \cdot mg = -L_f \cdot f_{ym} - L_T \cdot f_{yf} \tag{3.6}$$

Assuming the weight of the robot is mg at the center of mass of the body, the height h and the distances between the legs, i.e. L_f and L_T, are constant. Equation (3.6) is a linear equation in 2-variables (f_{ym} and f_{yf}). The two variables are inversely proportional to each other, i.e. in order to decrease one variable, the other one must increase. The optimum of minimizing the maximum of the two variables (adhesion) could be achieved by equating the two variables (f_{ym} and f_{yf}).

$$f_{ym} = f_{yf} \tag{3.7}$$

To facilitate the representation of the adhesion force, the two normal forces are represented as a positive value, acting in the direction of the negative y-axis. Let $f_{ym} = -F_{adh}$ and $f_{yf} = -F_{adh}$. Equation (3.6) could be rewritten as follows:

$$F_{adh} = (h \cdot mg)/(L_f + L_T) \tag{3.8}$$

The solution to the problem is redundant, as the optimal adhesion force, in Equation (3.8), is independent of the shear forces, i.e. f_{xf}, f_{xm}, and f_{xh}. In other words, the forces f_{xf}, f_{xm} and f_{xh} on the tips of the legs could have any value as long as they satisfy Equation (3.1). The redundancy of the solution is used in Chapter Seven to minimize the maximum torque on the joints of a climbing robot without compromising the optimal adhesion force.

3.4. Generalization

The solution to the problem of minimizing the maximum adhesion of a three legged robotic structure could be expanded to include structures with higher numbers of legs. Assuming that a robot has n middle legs, with a total of $(n+2)$ including the front and the hind legs, such as that shown in Figure 3.2, the equilibrium of forces equations are as follows:

$$\sum \boldsymbol{F_X} = \boldsymbol{f_{xf}} + \sum_{i=1}^{n} \boldsymbol{f_{xm_i}} + \boldsymbol{f_{xh}} - \boldsymbol{mg} = \boldsymbol{0} \qquad (3.9)$$

$$\sum F_Y = f_{yf} + \sum_{i=1}^{n} f_{ym_i} + f_{yh} = 0 \qquad (3.10)$$

$$\sum M_Z = h.mg - \sum_{i=1}^{n} \left(L_{f_i} \cdot f_{ym_i}\right) - L_T \cdot f_{yf} = 0 \qquad (3.11)$$

where f_{ym_i} and f_{xm_i} are the normal and the shear forces at the tip of the i^{th} middle leg respectively, and the L_{f_i} is the distance between the i^{th} middle leg and the hind leg.

Similar to the case of the three legged robot, the minimum adhesion is when the n legs undergo the same adhesion force value, which must satisfy $f_{ym_1} = f_{ym_2} = \cdots = f_{ym_n}$. Replacing the normal forces with one symbol, $f_{ym_i} = -F_{adh}$, where $i = 1,2,\ldots,n$, the optimal value of the normal adhesion force would be found using the following equation:

$$F_{adh} = (h \cdot mg)/(\sum_{i=1}^{n} L_{f_i} + L_T) \qquad (3.12)$$

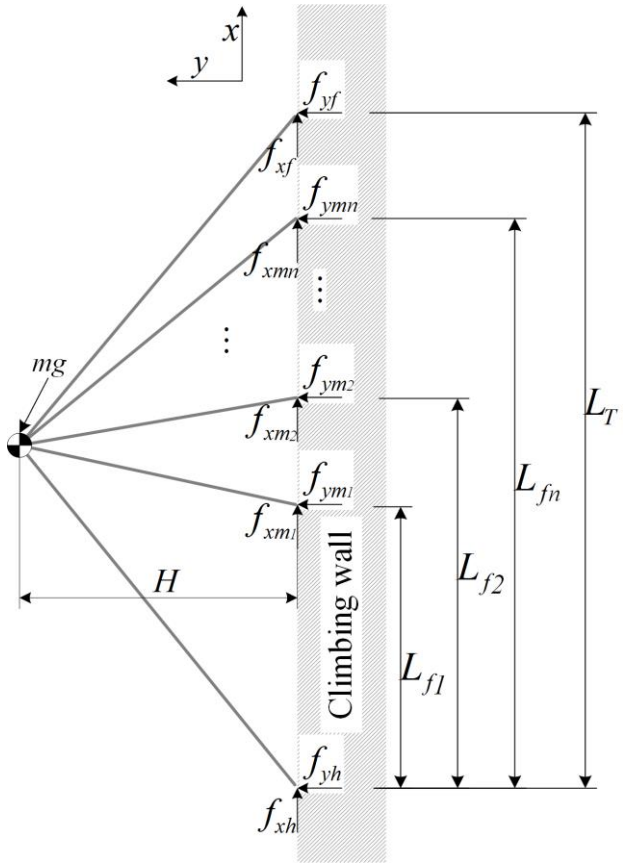

Figure 3.2. A robotic structure with $(n+2)$ legs

3.5. Discussion

The model used to calculate the optimal adhesion force assumes the legs to be weightless, and their weight is concentrated at the center of mass of the body. This assumption already considers the worst scenario as the center of mass of the whole robot is assumed to be at the highest point, i.e. the center of mass of the body. Consequently, the optimal normal adhesion force is higher than when considering the weight of the links of the legs to be distributed on their respective links. A higher center of mass generates larger moment on the body of the robot, which in turn causes the adhesion to be higher. Also, the model ignores the height of both the feet and the adhesion mechanism used to adhere to the vertical surfaces.

The equation of the maximum adhesion, Equation (3.12), minimizes the maximum adhesion. However, minimizing the sum of the normal adhesion forces on the tips of the legs, as shown in Equation (3.6), would concentrate the force on only one leg, i.e. the front leg, because the front leg in Equation (3.6) has the highest coefficient, as L_T is greater than L_f.

Chapter 4.

Adhesion optimization using variable stiffness materials

4.1. Introduction

In this chapter, the normal adhesion requirements are minimized by changing the elasticity of the legs. The change in elasticity is assumed to be utilized using variable stiffness materials. The robotic structure studied is simplified into 2-dimensional structure and analyzed using the finite elements method (FEM), specifically the stiffness method. FEM is used to calculate the reaction forces of the tips of the legs of the robot on climbing surfaces; which corresponds to the adhesion force required to keep the robot loitering on a vertical surface. The elasticity of the legs is presented in this chapter as a ratio to the body's elasticity to generalize the results for the usage of any material [80].

4.2. Robotic Model

Hexapod robots such as Digbot [12], Abigaille II [18] and Abigaille III [3] generally have an axis of symmetry parallel to the forward walking direction, shown in Figure 4.1. Such robots can be simplified and studied in 2-dimensions, as long as the left and the right parts of the robots are symmetric.

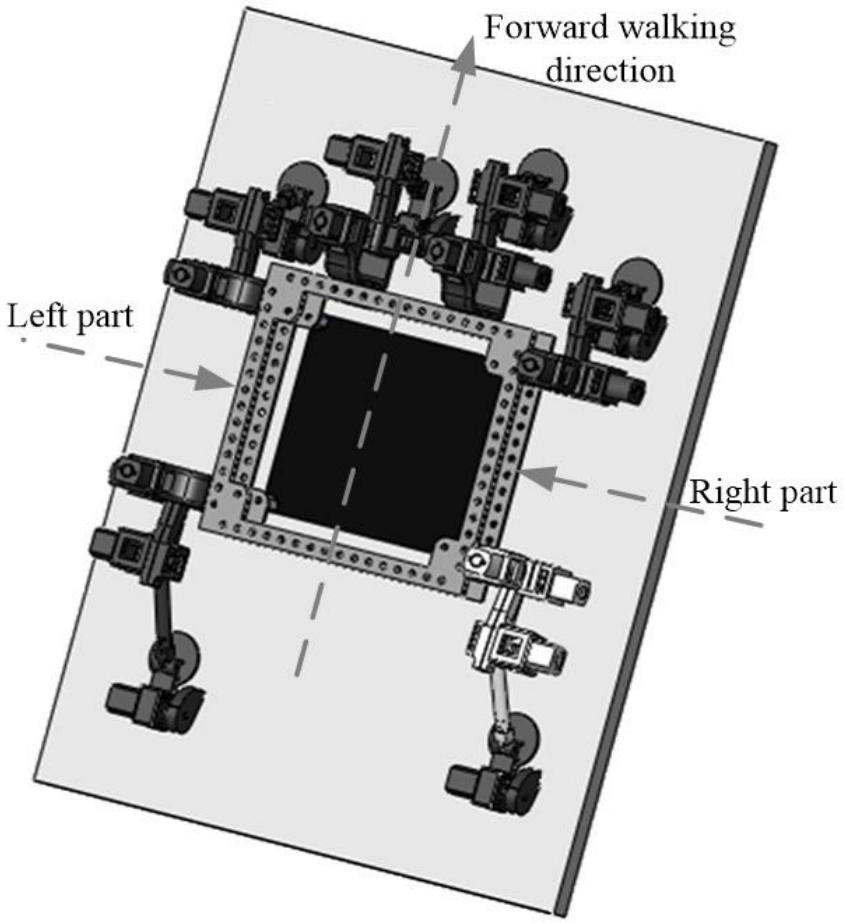

Figure 4.1. Abigaille III [3] walking upward of a surface.

The robot is considered to be loitering, as it is attached to the vertical surface. In this configuration, the motors of a robot would exert a constant torque on their legs to keep them in place and avoid detachment. From a quasi-static analysis perspective, each leg can therefore be considered as a part of a rigid structure. In order to simplify the analysis and draw conclusions that could be generalized to most six-legged robots, each robotic leg was arbitrarily simplified to be a straight equivalent beam. It should be noted that the effect of taking the weight of the legs into account without changing the overall weight of the robot would only slightly affect the shear and normal force distribution in the feet. Specifically, the shear forces would be more evenly distributed among the legs. The normal forces on the feet would instead slightly decrease given the center of mass of the robot would be closer to the surface. In this work, the weight of the robot is assumed to be equal to one unit in all of the performed calculations in order to

conveniently represent the forces on the tips of the feet as a percentage of the applied load. This normalization is used to generalize the results obtained in this work to a large variety of robots having different values of weight and dimensions. Figure 4.2 shows the simplified equivalent model that was considered. It should be noted that the legs of the robot were assumed to not transfer moment to the vertical surface, as commonly done in the literature [18], [19], [21], [22], [50], [81]–[84]. In this and the subsequent two chapters, the joints that connect the different straight links are referred as nodes, and the links are referred as beams.

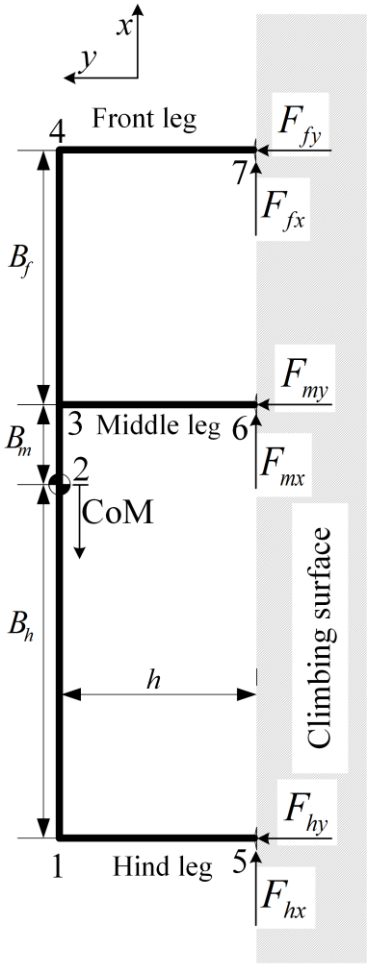

Figure 4.2. The 2D simplified model of Abigaille III [19]**.**

4.3. FEM Analysis

The robotic structure presented in the previous section is analyzed using FEM, specifically the stiffness method [51], which uses the beams' stiffness relations to compute the forces and the displacements of the structure. The overall relationship between the forces applied to the structure (axial loads, shear loads and bending moments) and the resulted displacements is given by:

$$\boldsymbol{F} = \boldsymbol{KD} \qquad (4.1)$$

where K is the structural stiffness matrix, F is a vector representing both the known forces applied to the structure and the unknown reaction forces of the nodes and D is a vector comprising the known and the unknown displacements of the nodes.

The structure of the robot is divided into 6 separate beams, see Figure 4.2. Specifically, three beams represent the legs. Specifically, one beam, connecting nodes 1 and 5, is the hind leg. A second beam, connecting nodes 3 and 6, is the middle leg. A third beam, connecting nodes 4 and 7, is the front leg. Additionally, a fourth beam is used to connect the hind leg, node 1, and the center of mass (CoM), node 2, a fifth beam connects the center of mass, node 2, with the middle leg, node 3, and a sixth beam connects the middle leg, node 3, with the front leg, node 4. The case when the middle leg is located between the hind leg and the center of mass is also formed using six beams. The only difference is that the front leg is directly connected to the CoM using a beam, and the hind leg is connected to the middle leg using a beam.

The known displacements are those of the constrained nodes, namely those of the hinges (H_h, H_m, H_f) in *x* and *y* axes (see Figure 4.2), are equal to zero. The unknown degrees of freedom are the distance the unconstrained nodes moved after applying the known forces on the structure; from Figure 4.2, the unknown degrees of freedom are the linear movement of nodes 1, 2, 3 and 4, and the rotation movement of all of the nodes, namely nodes 1, 2, 3, 4, 5, 6 and 7. The known forces are the weight of the robot at the center of mass, and the linear force components of all of the unconstrained nodes, namely nodes 1, 2, 3 and 4 along with the moment on all of the nodes, namely nodes 1, 2, 3, 4, 5, 6 and 7, are equal to zero. The unknown forces are the reaction forces at the

hinges, namely $F_{hx}, F_{hy}, F_{mx}, F_{my}, F_{fx}$ and F_{fy}, which are shown in Figure 4.2. Equation (4.1) can therefore be written as:

$$\begin{bmatrix} \boldsymbol{F_k} \\ \boldsymbol{F_u} \end{bmatrix} = \begin{bmatrix} \boldsymbol{K_{11}} & \boldsymbol{K_{12}} \\ \boldsymbol{K_{21}} & \boldsymbol{K_{22}} \end{bmatrix} \begin{bmatrix} \boldsymbol{D_u} \\ \boldsymbol{D_k} \end{bmatrix} \quad (4.2)$$

where $\boldsymbol{F_k}$ is the vector of the known forces, $\boldsymbol{F_u}$ is the vector of the unknown forces, $\boldsymbol{D_u}$ is the vector of the unknown displacements and $\boldsymbol{D_k}$ is the vector of the constrained displacements.

From Equation (4.2) , the unknown displacements $\boldsymbol{D_u}$ can be calculated as follows:

$$\boldsymbol{D_u} = \boldsymbol{K_{11}^{-1}} \cdot \boldsymbol{F_k} - \boldsymbol{K_{11}^{-1}} \cdot \boldsymbol{K_{12}} \cdot \boldsymbol{D_k} \quad (4.3)$$

The unknown forces, that are the reaction forces between the tips of the legs and the climbing surface, are calculated using:

$$\boldsymbol{F_u} = \boldsymbol{K_{21}} \cdot \boldsymbol{D_u} + \boldsymbol{K_{22}} \cdot \boldsymbol{D_k} \quad (4.4)$$

Substituting Equation (4.3) into Equation (4.4) yields:

$$\boldsymbol{F_u} = \boldsymbol{K_{21}} \cdot \left[\boldsymbol{K_{11}^{-1}} \cdot \boldsymbol{F_k} - \boldsymbol{K_{12}} \cdot \boldsymbol{D_k}\right] + \boldsymbol{K_{22}} \cdot \boldsymbol{D_k} \quad (4.5)$$

The known distances $\boldsymbol{D_k}$ are the displacements of the constrained nodes which are equal to zero; as such, the above equation can be rewritten as:

$$\boldsymbol{F_u} = \boldsymbol{K_{21}} \cdot \boldsymbol{K_{11}^{-1}} \cdot \boldsymbol{F_k} \quad (4.6)$$

Equation (4.6) is a closed form equation to calculate the reaction forces. Such an equation is implemented on a code developed in MATLAB environment. It should be noted that the force distribution depends on the stiffness of each beam relative to the other beams and not to the absolute stiffness value of each beam (see Appendix A). Therefore, the results obtained in this work can be generalized to robots having any

material and stiffness. Also, the lengths of the different beams are unit less and applicable to bigger and smaller structures.

Commercially available finite element method (FEM) software, i.e. ANSYS (V14.0), is used to verify the correct implementation of the stiffness method. Specifically, the beam element BEAM188 based on Timoshenko beam theory is used to analyze 2D structures [85]. The MATLAB code is tested against the ANSYS software by comparing randomly selected cases solved using MATLAB with the same cases solved using ANSYS.

4.4. Elasticity Investigation

This section presents the procedure used to investigate the effect of changing the elasticity for the different legs. The FEM used in the analysis, presented previously, is used to show the effect of changing the elasticity of the legs. The robotic structure assumes the height (h) to equal 100, and the length of the body $\left(B_f + B_m + B_h\right)$ to equal 200. All the measurements are dimensionless so the system could be scaled to bigger and smaller sized structures. The weight of the robot is considered to be applied at the center of mass and is equal to one in order to present the forces on the tips of the legs as a scale per one unit of the weight of the robot; for example, the forces at different weight, assumed to be w_d, equals the forces at unit weight times the weight of the robot w_d.

Investigating the legs' elasticity is done by changing the elasticity of two legs at a time depending on the location of the middle leg. The effect of changing the elasticity of the middle and the front legs are investigated when the middle leg is located at the front half of the robot, see Figure 4.3. While the effect of changing the elasticity of the middle and the hind legs is investigated when the middle leg is in the rear half of the robot, see Figure 4.3.

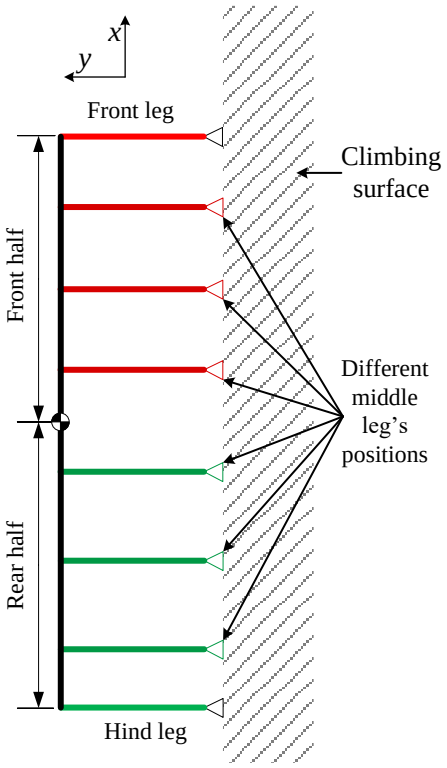

Figure 4.3. The stiffness of the hind and the middle leg is varied when the middle leg lies in the rear half, highlighted in green. The stiffness of the front and the middle leg is varied when the middle leg lies in the front half, highlighted in red.

4.4.1. Stiffness Change for the Middle and Hind Legs

The elasticity for the middle and the hind legs are varied while keeping the elasticity of both the front leg and the body fixed at 1, and the maximum adhesion is recorded. Figure 4.4 shows the maximum adhesion for different middle and hind legs' elasticity values at middle leg's position of 0.15, chosen arbitrarily, of the total distance between the hind and the front legs. A middle leg's position of 0 means that the middle leg is positioned at the hind leg and a position of 1 means that the middle leg is positioned at the front leg. The maximum values are shown as a curve highlighted in magenta, call it optimal elasticity curve. It corresponds to elasticity values where any elasticity values outside of that curve will require higher maximum adhesion force than the force resulted from using elasticity values on the optimal elasticity curve. It is worth mentioning that the adhesion value of the optimal elasticity curve is the absolute optimal

force value which is the same value if Equation (3.8) is used to calculate the optimal force.

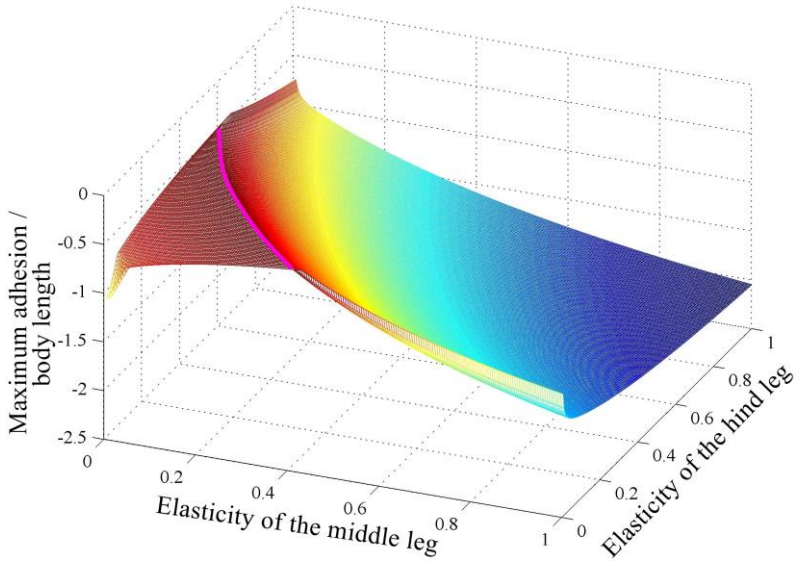

Figure 4.4. The maximum adhesion force required for different stiffness values of middle and hind legs' stiffness values. The optimal elasticity curve is highlighted in magenta.

The optimal elasticity curve for different middle leg's positions, placed between the hind leg and the center of mass, is shown in Figure 4.5. The colored lines represent the normalized different middle leg's positions. For example, selecting the optimal elasticity values for the middle and front legs for a middle leg position of 0.36, showed as a dashed line in Figure 4.5-b, of the total body length could be achieved by selecting any value on the corresponding curve, the dashed red line in Figure 4.5-b.

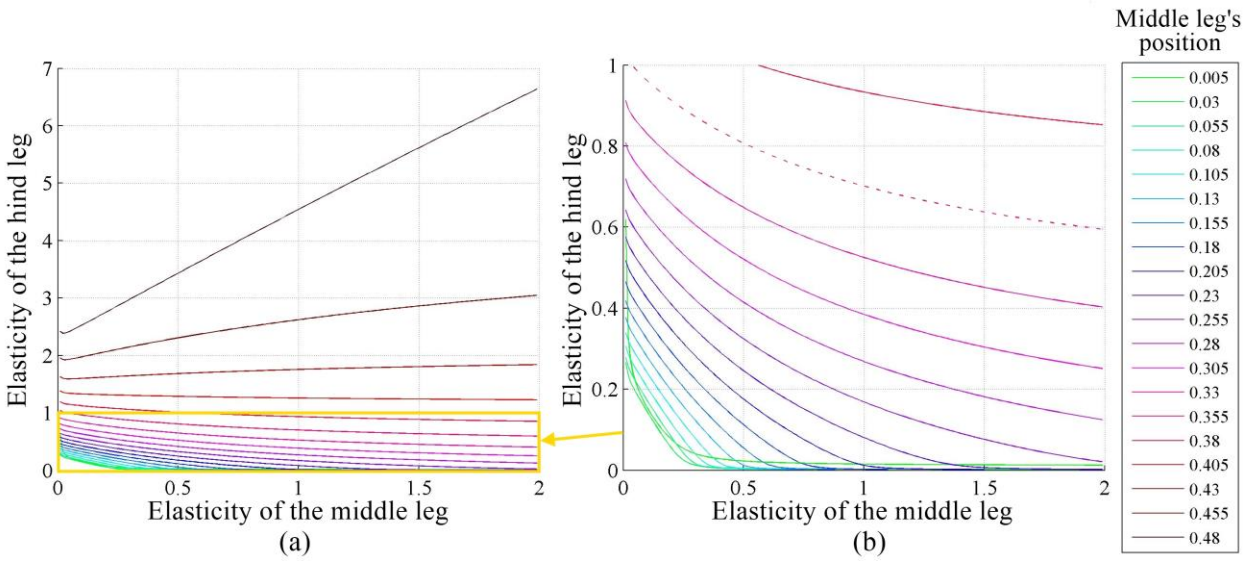

Figure 4.5. Optimal elasticity curves for different middle leg's positions. (b) is a zoomed in view of (a)

4.4.2. Stiffness Change for the Middle and Front Legs

The same procedure, used in the previous sub-section is followed here to find the curves of optimal elasticity for the positions of the middle leg located between the middle and the front legs. The elasticity values for the middle and the front legs that allow the robotic structure to use the optimal adhesion are shown in Figure 4.6. The range of the elasticity, which provides the optimal adhesion force, for the middle leg is bounded between 0 and 0.5 for any front leg's elasticity value.

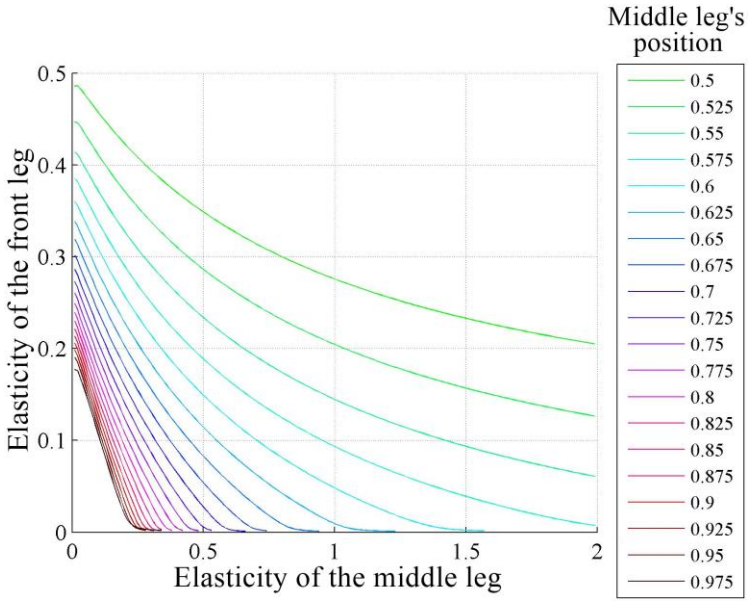

Figure 4.6. Optimal elasticity curves for different middle leg's positions.

4.5. Discussion

The improvement in the adhesion force requirement is a result of distributing the load on the front and the middle legs evenly by changing the elasticity of the legs. In Figure 4.4 for example, changing the elasticity of the hind and the middle legs to the optimal value, improves the required maximum adhesion force over 4 times compared to using legs with elasticity equals to that of the body's. The studied robotic structure has a height of 100 and a body length of 200 which has an aspect ratio of 1:2. This investigated case represents the exact behaviour of structures with any dimension as long as it has a height to length aspect ratio of 1:2 and the same second moment of area as the one with the height of 100 and the length of 200.

The behaviour of climbing robots with different structures is similar to the investigated case. Specifically, varying the elasticity of the hind and the middle legs improves the adhesion force requirement when the middle leg is positioned in the rear half of the robot; while varying the elasticity of the middle and the front legs improves the adhesion force requirement when the middle leg is positioned in the front half of the robot. The optimal adhesion values, which corresponds to the value of the optimal

elasticity curves, are the same as using Equation (3.8) to calculate the values of the optimal adhesion or the specific height and legs' tip positions.

This chapter considers robots with single straight beams. The effect of the geometrical shape of the legs is not included in the FEM analysis. Multi-beam legs are essential as they are required in order for the robot to move along the vertical surface. However, the optimal adhesion force would be attainable for any structure with multi-beam legs by varying the stiffness of the legs.

Chapter 5.

Adhesion Optimization by Changing the Geometry

5.1. Introduction

In this chapter, a number of parameters, namely the (1) height of the robot, the (2) length of its body, the (3) position of its legs, the (4) thickness of the beams forming the robot, and the (5) body and the (6) legs' inclination, are investigated to assess their effect on the adhesion requirements needed for the robot to stay attached to a wall. Predictions of the developed mathematical model are validated using ANSYS, a FEM commercial software [86], [87].

In order to simplify the analysis and draw conclusions that could be generalized to most six-legged robots, similar to the simplifications carried in the previous chapter, each robotic leg was arbitrarily simplified to be a straight equivalent beam, with stiffness approximately equal to that of the robotic leg. In order to account for the different possible values of stiffness that different robots or different leg's configurations could have, the cross-section area of the equivalent beam is varied. A similar consideration was done for the body of the robot, which was also modeled with a straight beam and whose stiffness was changed by changing its cross-section area. By considering the legs and body to be weightless and assuming the mass of the robot to be concentrated at its center of mass (CoM), which is consistent with the existing literature [18], [19], [21], [22], [42], [50], [82], [83], [88], the variation of the cross-section area did not affect the weight of the robot and a comparative analysis was therefore possible.

The FEM method presented in the previous chapter is used in this chapter also to minimize the normal adhesion required by the robot to stay attached to a vertical surface, i.e. F_{hy}, F_{my} and F_{fy} in Figure 4.2. The adhesion considered here is dry

adhesion, although other adhesion types could be considered. The normal force adhesion is investigated by examining different geometrical parameters of the simplified robotic structure.

For structures with infinite stiffness, only the height to body length ratio and the middle leg's position are studied. The shape of the beams, and the body and legs' inclinations are not taken into account as they have no effect on such structure.

5.2. Effect of Height to Length Ratio and the Middle Leg's Position

In this section, the effect of the height to length ratio and the position of the middle leg on the maximum adhesion are studied in this section. The case when the structure of the climbing robot has a finite stiffness is presented first, while the case when the structure has an infinite stiffness is presented second.

5.2.1. Finite stiffness structure

This section describes the effect of changing the body height to body length aspect ratio and the effect of the position of the middle leg on the adhesion force requirement on the tips of the legs. For the robot shown in Figure 4.2, B_f is the distance between the middle and the front legs, $(B_m + B_h)$ is the distance between the middle and the hind legs and h is the height of the robot. The length of the body, $\left(B_f + B_m + B_h\right)$, is arbitrarily chosen to be 200, while the radius of the beams are assumed to be the same and equals to two, and the height is in the 2.1-2000 range, which corresponds to a range of height to body length ratio of 0.0105-10. The obtained results are applicable to both bigger and smaller structures as long as the ratio of the height to the length is within the range and the radius is kept fixed. Distribution of the calculated normal force, representing the adhesion force requirement, for the change in the height to length aspect ratio and the position of the middle leg is shown in Figure 5.1. Three different configurations are compared with ANSYS and plotted over the curve (see circles in Figure 5.1) obtained by using MATLAB. The average error between simulations performed in MATLAB and ANSYS is 0.61%.

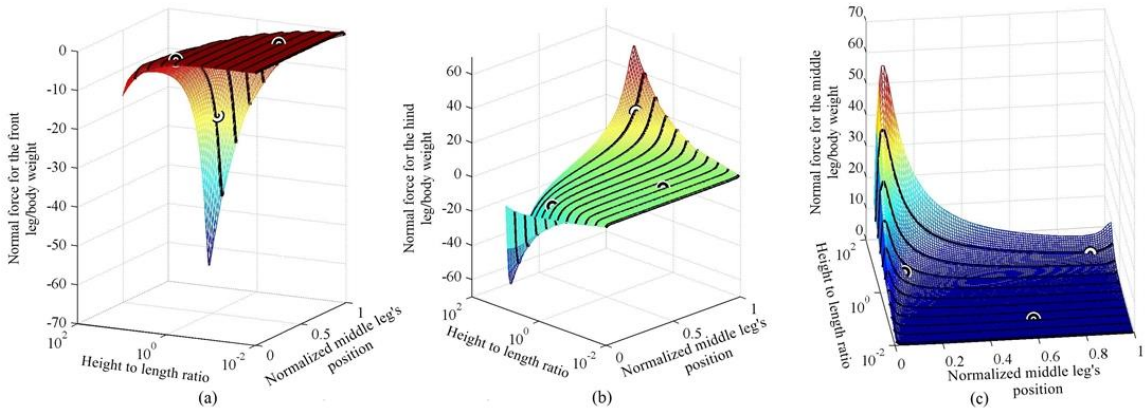

Figure 5.1. Shows the required normal force at different height to length aspect ratio and different middle leg's positions for (a) front leg, (b) middle leg and (c) hind leg. Circles represent simulations performed using ANSYS.

The x-axis in Figure 5.1 represents the position of the middle leg, where 0 means that the middle leg is positioned at the back of the robot. In this configuration the middle leg has the same position as the hind leg. The value of the x-axis increases as the middle leg gets closer to the front leg and the value equals 1 when the middle and front legs have the same position. The y-axis represents the height to length aspect ratio and the z-axis represents the normal force per body weight. From Figure 5.1, increasing the body height to body length ratio, on the x-axis, requires higher force to keep the robot attached to the vertical surface because, a robot with higher height and fixed weight causes an increase in the torque applied to the robot's structure due to gravity which needs higher forces on the tips of the legs to keep the robot in equilibrium than that required by a robot with lower height.

The normal force in Figure 5.1 has 2 peaks located at middle leg positions of 0.07 and 0.93; the first peak is located at the hind leg with a maximum of 64.16 and the second is located at the middle leg with a maximum of 56.66. The peaks can be explained by analyzing the shear and normal forces distributions for a specific robotic structure with fixed height to length aspect ratio. The shear force distribution due to changing the middle leg's position and the normal force distribution resulting from changing the middle leg's position are explained in Appendix B.

The design that requires the least adhesion force for a robot with parallel body and perpendicular to the climbing surface legs can be found from Figure 5.1. The maximum adhesion needed by any of the legs at different heights and different middle leg's positions is shown in Figure 5.2. An optimization is performed to identify the optimal height and middle leg's position of the robot; the optimal structure found has an optimal height of 2.1 and an optimal middle leg's position at 0.335.

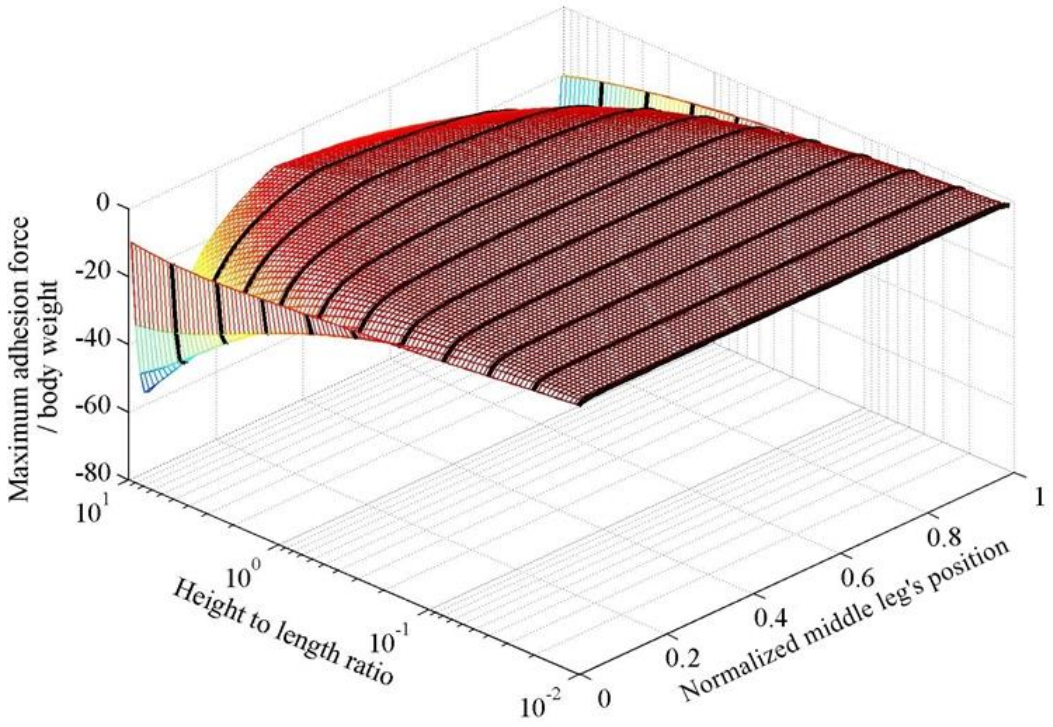

Figure 5.2. The maximum adhesion force for different height to length ratios and different middle leg's positions

The optimizer is configured to search for the optimal middle leg's position within the range of 0 to 0.95 in order to prevent the optimizer from converging to the global optimum at 1. In fact, the global optimum is not considered to be the most desirable value as a small variation from the minimum causes a dramatic increase in the adhesion requirement. In fact, in Figure B.3, a small variation of the leg from its optimal position causes the maximum adhesion requirement to increase dramatically. For example, a 0.01 variation in position causes a more than 250 fold increase in the required adhesion.

It should be noted that the 2.1 is the smallest height that is considered in this study. In fact, the radius of the structure is assumed to be two and a minimum gap between the robot and the surface is assumed to be 0.1. As expected, it can be concluded that the height should be as low as possible.

5.2.2. Infinite stiffness structure

The effect of the height, the length of the structure and the middle leg's position on the maximum normal adhesion for infinite stiffness structures is presented here. Equation (3.8) is used in this section to show the effect of the three parameters, on the maximum adhesion on the tips of the legs. In Equation (3.8), let $L_f = c \cdot L_T$, where $0 \leq c \leq 1$, as the position of the middle leg is always between the front and the hind leg which could be presented as a fraction. $c = 0$ when the middle leg is positioned at the farthest back, i.e. the same position as the hind leg, as c increases the middle leg's position gets closer to the front. $c = 1$ is when the middle leg is positioned at the most front, i.e. the middle leg has the same position as the front leg. The equation could be rewritten as follows:

$$F_{nf} = mg \cdot h/(L_T \cdot (1 + c)) \qquad (5.1)$$

The equation shows that the maximum adhesion is directly proportional to the height and inversely proportional to the length of the robot. The position of the middle leg c, i.e. the distance between the middle and the front legs, is inversely proportional with the maximum adhesion.

Using the results obtained here is not possible on robots with position controlled motors as there is no infinite stiffness materials that could be used to build a climbing robot. However, these results are applicable to robots with force/torque control implemented on their feet.

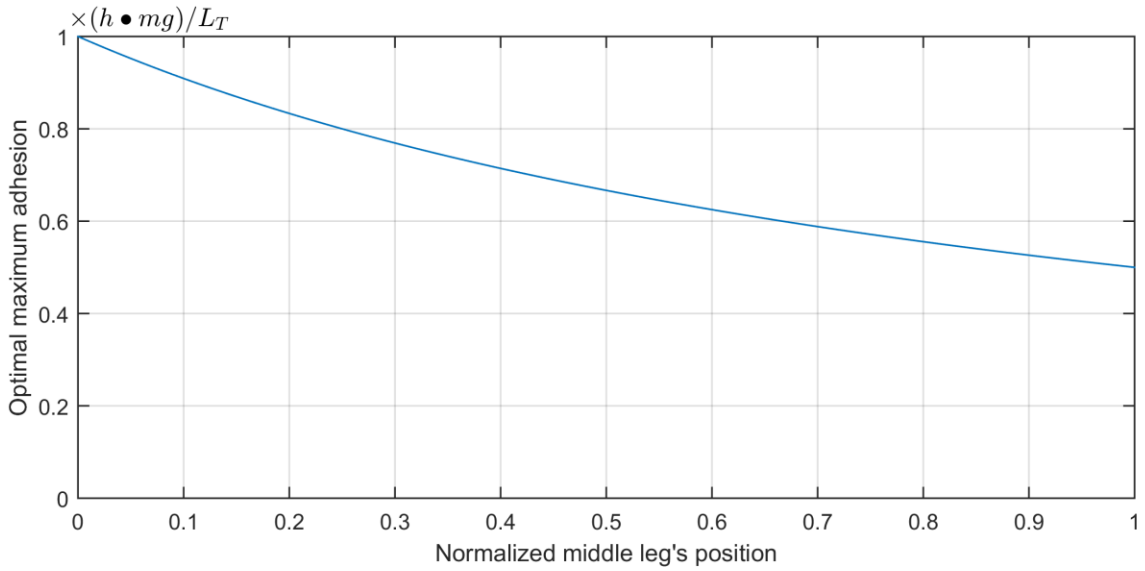

Figure 5.3. The optimal maximum adhesion force required on the tips of the legs

5.3. Effect of Body and Legs Thickness

The change in the cross sectional area is investigated to cover a change in the stiffness of the legs. As changing the radius of the legs shows a similar effect to changing the stiffness of the legs; the greater the cross sectional area is, the greater the legs' resistance to compression and torsion.

A structure with body length of 200 and a height of 100 is arbitrarily chosen to explore the effect of changing the cross sectional area on the normal force distribution of a robot. Results drawn from this specific geometry are generalized in a subsequent section.

The cross sectional area and the area moment of inertia are varied, while the weight of the robot is considered to be fixed at one and applied at the center of mass. The area moment of inertia is calculated to be equivalent to that of a circle; the radius is calculated from the cross sectional area, and the area moment of inertia is then calculated accordingly. The normal force distribution is calculated for different cross sectional area values for the legs, between 0.0001 and 3.16×10^4, while keeping the cross sectional area of the body, formed by the horizontal beams in Figure 4.2, fixed at

one. It has similar effect to changing the stiffness of the legs while keeping the stiffness of the body fixed. The normal force required for each leg to stick on the wall for different legs' cross sectional area and middle leg's position is shown in Figure 5.4. Three different configurations are compared with ANSYS and plotted over the curve obtained in Figure 5.4; the test points have an average absolute error of approximately 2%.

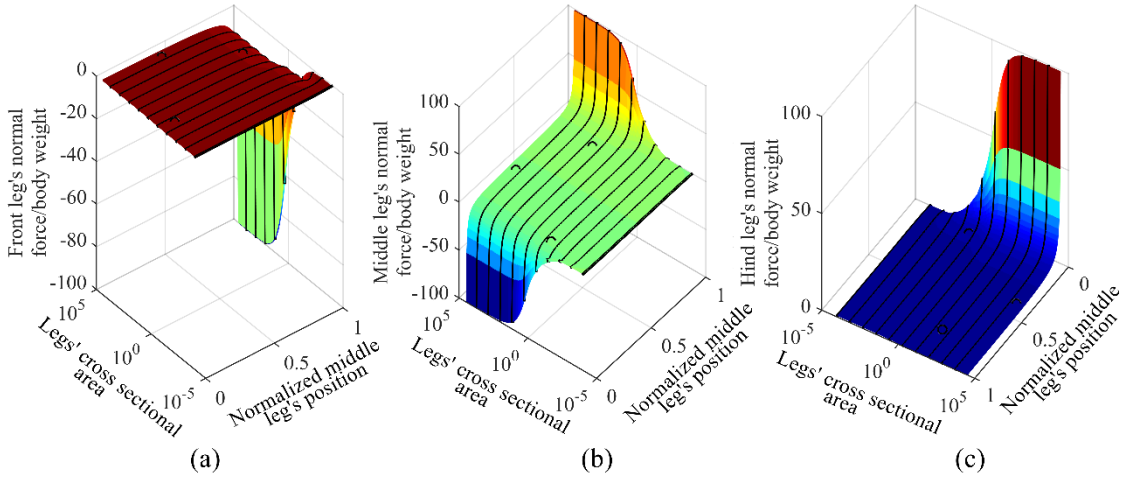

Figure 5.4. Normal forces required by the feet of the robot for different legs' cross sectional areas and different middle leg's positions with the body's cross sectional area fixed at 1. Circles represent simulations performed using ANSYS.

The range of the cross sectional area in Figure 5.4 is selected to be from 0.0001 to 3.16×10^4. Simulations performed considering the values of the cross sectional area outside this range showed that variation of the cross sectional area had little effect (variation smaller than 0.01%) on the force distribution. The three sub-figures in Figure 5.4 are combined to show the minimum normal forces among the front, middle and hind legs in Figure 5.5, which represents the maximum adhesion required to keep the robot attached to the wall.

The best position for the middle leg, in the range between 0 and 0.99, is located between 0.3 and 0.42 for the range of legs' cross sectional area from 0.045 to 100, while the best range for smaller cross sectional area, less than 0.045, jumps to be at 0.99, see Figure 5.5-b. For any cross sectional area, the best position of the middle leg is when it overlaps the front leg, i.e. the middle leg has a position equals to one for any cross sectional area value.

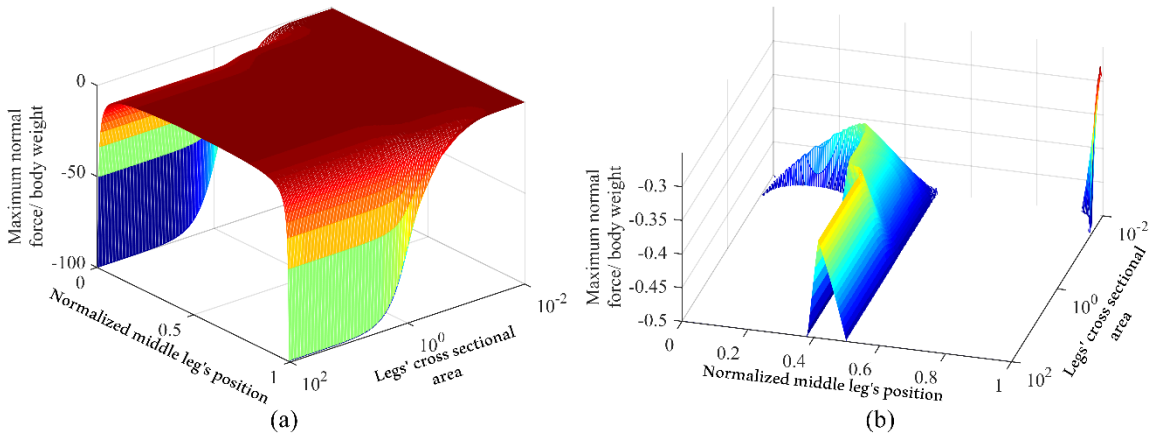

Figure 5.5. Shows, for a range of values of legs' cross sectional area and middle leg's positions (a) Maximum adhesion force requirement, (b) maximum adhesion force within -0.5 and -0.1 of the maximum normal force/body weight.

In summary, the optimal configuration when the body is parallel and the legs are perpendicular to the vertical surface is when the structure has a minimum legs' cross sectional area of 0.0001 and a middle leg's position of 0.99. Changing the body's cross sectional area and fixing the legs' cross sectional area has an opposite adhesion force requirement behavior to that shown in Figure 5.4; the lowest point of the graph is when the body cross sectional area is at minimum, which equals 10^{-4}, and the maximum point is when the radius at maximum, which equals 3.16×10^4.

5.4. Effect of Body Inclination

The robot considered in this section is also assumed to have a height to body length ratio of 1:2. Results drawn from this specific geometry are generalized in a subsequent section.

Using a robot with height to body length ratio of 1:2 implies that collision occurs when the body inclination is either over 45^o or less than -45^o, where 0^o inclination is defined when the robot's body is parallel to the climbing surface (see angle θ_B in Figure 5.6). The height and the distance between the front and the hind legs are considered to

be fixed to keep the height to length ratio fixed at every inclination, see Figure 5.6. As discussed earlier, no units are used, as the results can be scaled up/down.

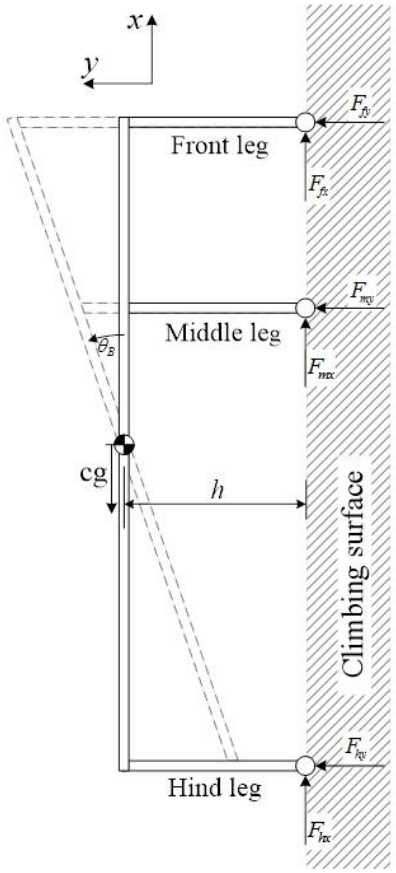

Figure 5.6. Robotic structure with a body inclination angle of θ_B.

The effect of changing both the position of the middle leg and the inclination of the body is shown in Figure 5.7. Three different configurations are compared with ANSYS and plotted (see circles) over the curve obtained by using MATLAB in Figure 5.7, with an average error of approximately 1.29%.

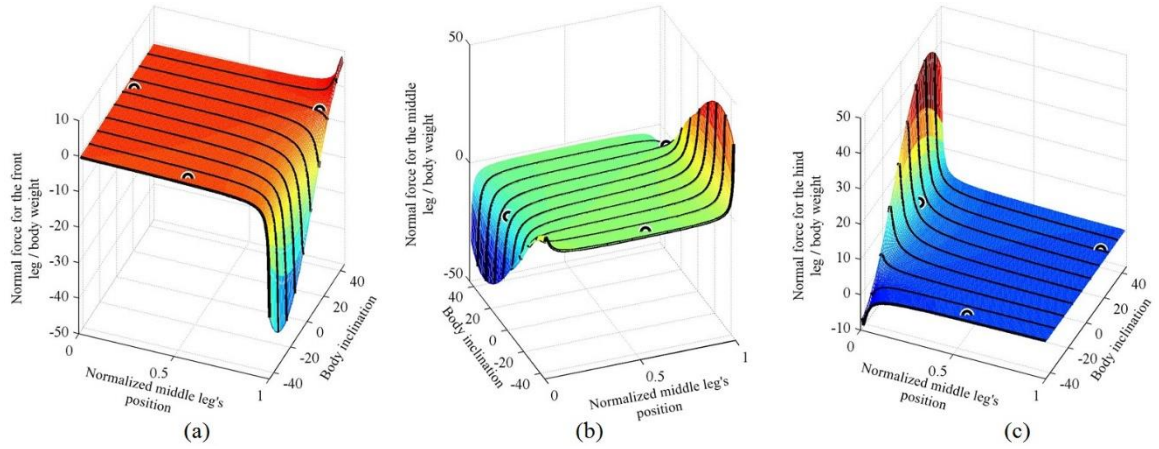

Figure 5.7. Shows the normal forces for different body angles and different middle leg's positions for (a) front leg, (b) middle leg, (c) hind leg. Circles on the plot represent simulations performed using ANSYS.

The maximum adhesion force required by each leg for the different angles of the body is shown in Figure 5.8. The optimal structure in Figure 5.8 is found to have a body angle of approximately 28.25^{o} and a middle leg's position of 0.99, where the middle leg's position is bounded in the 0.01-0.99 range.

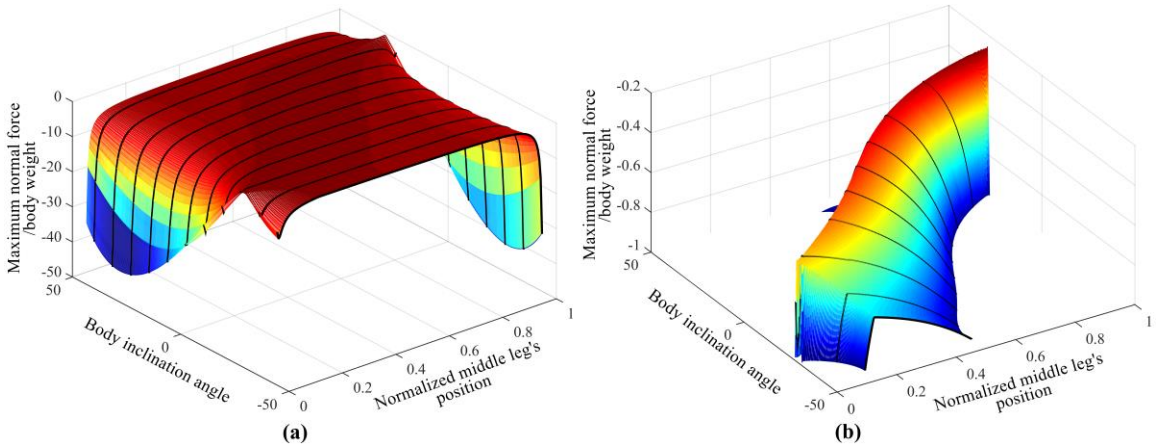

Figure 5.8. The maximum adhesion force required by any foot for different body angles and different middle-leg positions.

The inclination of the body by a positive angle θ_B (counter clockwise angle in Figure 5.6) causes the beams of the front half body of the robot to become longer and therefore more flexible, whereas the beams on the hind half body (see Figure 5.6) to become shorter and therefore stiffer. A negative body inclination angle causes an

opposite effect. In other words, the body inclination affects the stiffness of the different parts of the robot. This general behavior can be generalized to robots having different height to length ratios. It should be noted that a robotic structure with a smaller height to length aspect ratio would have a smaller inclination range, thus limiting the choice of optimal body inclinations.

5.5. Effect of Legs Inclination

The effect of having the legs inclined instead of perpendicular to the climbing surface is investigated in this section. Similar to the previous sections, the adhesion force required to keep the robot on a perpendicular surface is assumed to be minimized.

The robot's structure is the same as that used in the previous section (assumes a body length of 200 and a height of 100). The legs are arranged so they are inclined outward, i.e. the front leg is inclined forward and the hind leg is inclined backward to mimic climbing arthropods such as ants, cockroaches, and spiders. In this section two cases for the middle leg are considered. In the first case, the middle leg is inclined towards the front of the robot with inclination angle equals to the front leg's inclination (see the solid lines in Figure 5.9). While, in the second case, the middle leg is inclined towards the back of the robot with inclination angle equals to the hind leg's inclination (see dashed lines in Figure 5.9). Figure 5.9 shows a diagram of a robot, where d_B is the length of the body, d_T is the distance between the tip of the front leg and the tip of the hind leg which is kept fixed at 200, the angles of the front, the middle, and the hind legs make $(\theta_f, \theta_m$ and $\theta_h)$ respectively with the body.

The range of the front leg's angle is from -90^o to -45^o, and the hind leg's angle to range from -135^o to -90^o. At the maximum inclination, i.e. $\theta_f = \theta_m = -45^o$ and $\theta_h = -135^o$, all of the three joints are located at the center of mass. A wider inclination range at this height is not feasible without increasing the distance between the tips of the front and the hind legs.

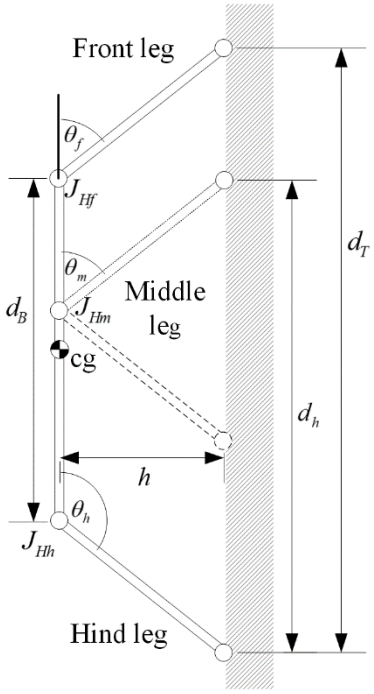

Figure 5.9. Shows the robot with the inclined legs.

The case when the middle leg's inclination equals the front leg's is considered first. An inclination angle θ_{inc} is introduced to represent the inclination of the legs. All the legs are perpendicular to the climbing surface at $\theta_{inc} = 0^o$, and the front and the middle legs have a -45^o angle with the body and the hind leg has -135^o with the body at $\theta_{inc} = 45^o$. The angle of the front and the middle legs can be represented using the following equation:

$$\theta_f = \theta_m = -90 + \theta_{inc} \quad (5.2)$$

The hind leg's angle can be represented as a function of θ_{inc} as follows:

$$\theta_h = -90 - \theta_{inc} \quad (5.3)$$

The normal force distribution for the range of θ_{inc} with different middle leg positions is shown in Figure 5.10. Three different configurations are compared with ANSYS and plotted over the curve obtained by using MATLAB, with an average error of approximately 0.14%. The position of the middle leg's joint (J_{Hm}) is represented as a fraction of the distance d_T where the value 0 is positioned at the hind leg's tip and 1

being at the front leg's tip. The curves of the different legs' positions have different lengths, because the range available for the hip position of the middle leg decreases as the angle θ_{inc} increases.

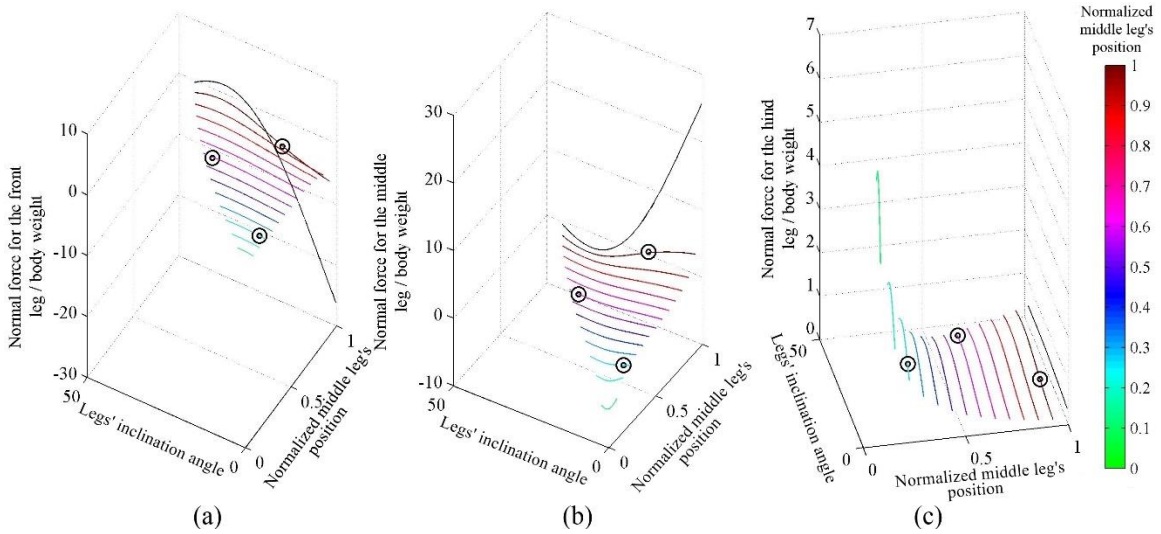

Figure 5.10. The normal force distribution with the middle leg inclines forward for different θ_{inc} values and different middle legs' positions, on (a) the front leg, (b) the middle leg and (c) the hind leg. Circles represent simulations performed using ANSYS.

The maximum adhesion force applied by the robot to the vertical surface can be identified by analyzing Figure 5.11, which combines the three subplots of Figure 5.10. It can be noted that inclining the middle leg forward improves the adhesion requirement when the position of the middle leg is greater than 0.38 (see red circle and legend in Figure 5.11-b). Bringing the middle leg closer to the front leg, with the optimal inclination for that position, results in requiring less adhesion force.

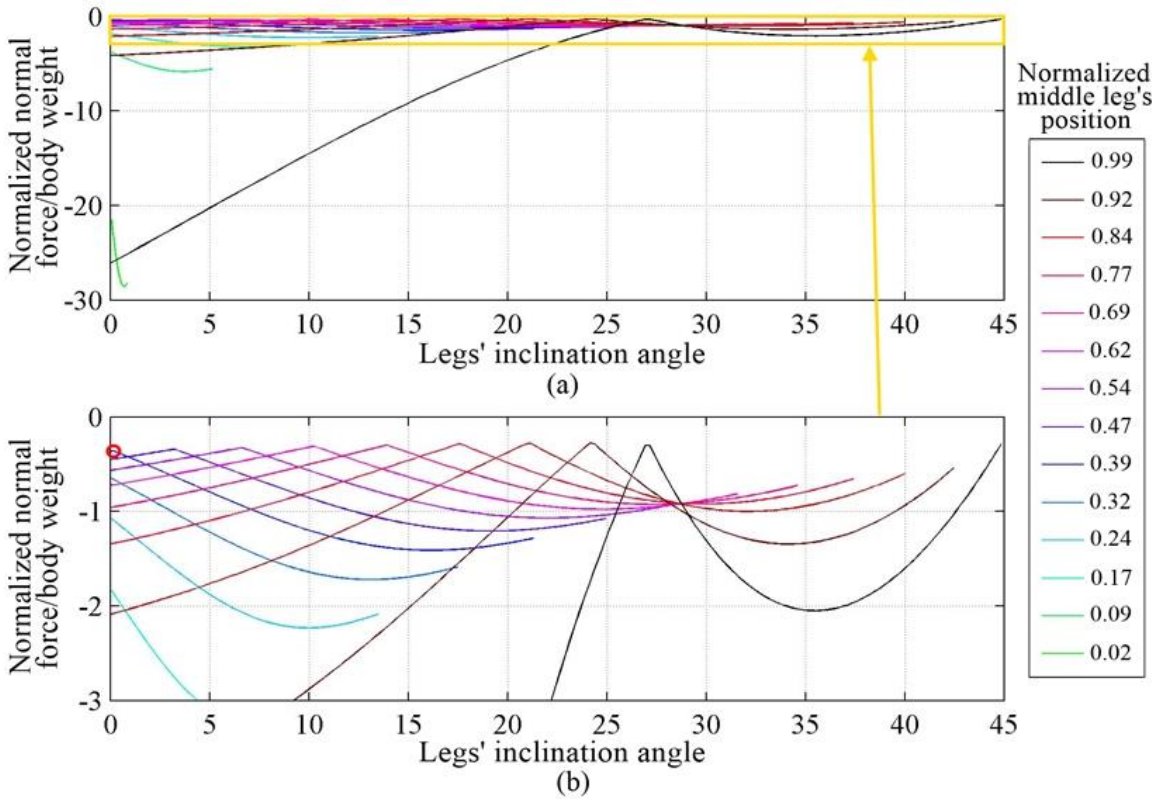

Figure 5.11. (a) The maximum adhesion required by the robot at different legs' inclinations and different middle leg's positions. (b) Zoomed in view of plot (a). The red circle in (b) shows the closest middle leg's position to the hind leg that improves with forward inclination of the middle leg.

The case when the middle leg inclines backward, i.e. has the same inclination angle as the hind leg's angle, is investigated similar to the previous case; an inclination angle θ_{inc} is used to represent the inclination of the legs. The equation of the inclination angle for both the front leg, Equation (5.2), and the hind leg, Equation (5.3), are the same as in the previous case; while the inclination angle for the middle leg is the same as the hind leg's equation, i.e. Equation (5.3). The normal force distribution for the range of θ_{inc} with different middle leg positions is shown in Figure 5.12. Three different configurations are compared with ANSYS and plotted over the curve obtained by using MATLAB, the circles in Figure 5.12, in which they have an average error of approximately 0.13%.

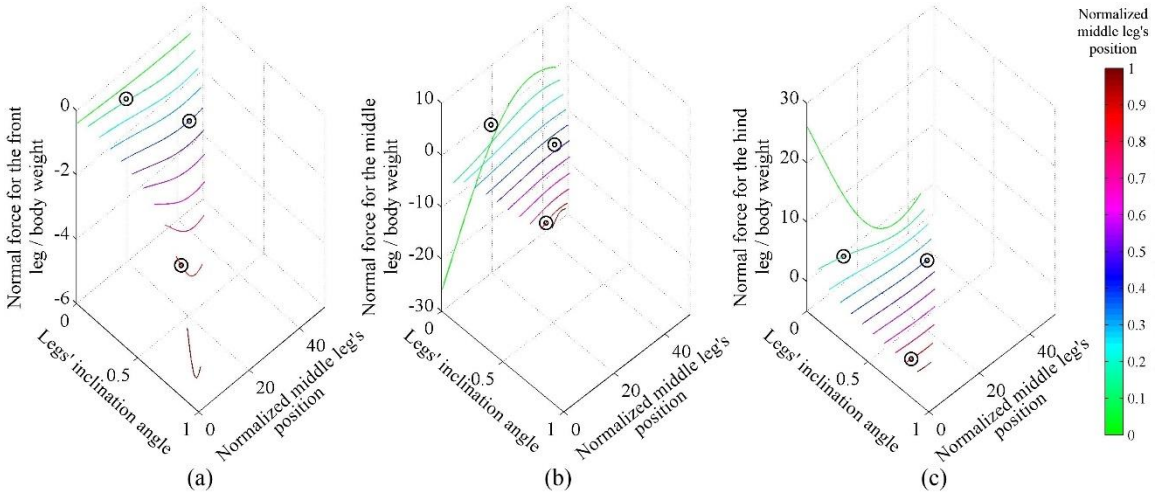

Figure 5.12. The normal force distribution on the legs of the robot for different legs' inclinations and different middle legs' positions on (a) the front leg, (b) the middle leg and (c) the hind leg, with the middle leg inclined backward. Circles represent simulations performed using ANSYS.

The maximum adhesion force required for all of the configurations is constructed by combining the three sub-Figures of Figure 5.12, and their plot is shown in Figure 5.13. The lower plot in Figure 5.13 is a zoom of the upper plot in Figure 5.13.

From Figure 5.13, the backward inclination of the legs improves the adhesion requirement when the middle leg's position is below 0.38 (see red circle in Figure 5.13-b). The backward legs' inclination for any other position will cause an increase in the required force. The effect of legs' inclination for different height to length ratios has the same effect as the investigated structure with 1:2 height to length aspect ratio. With the exception that the point that improves with the backward legs inclination is varied to be between 0.38 and 0.41 for the range of heights considered earlier.

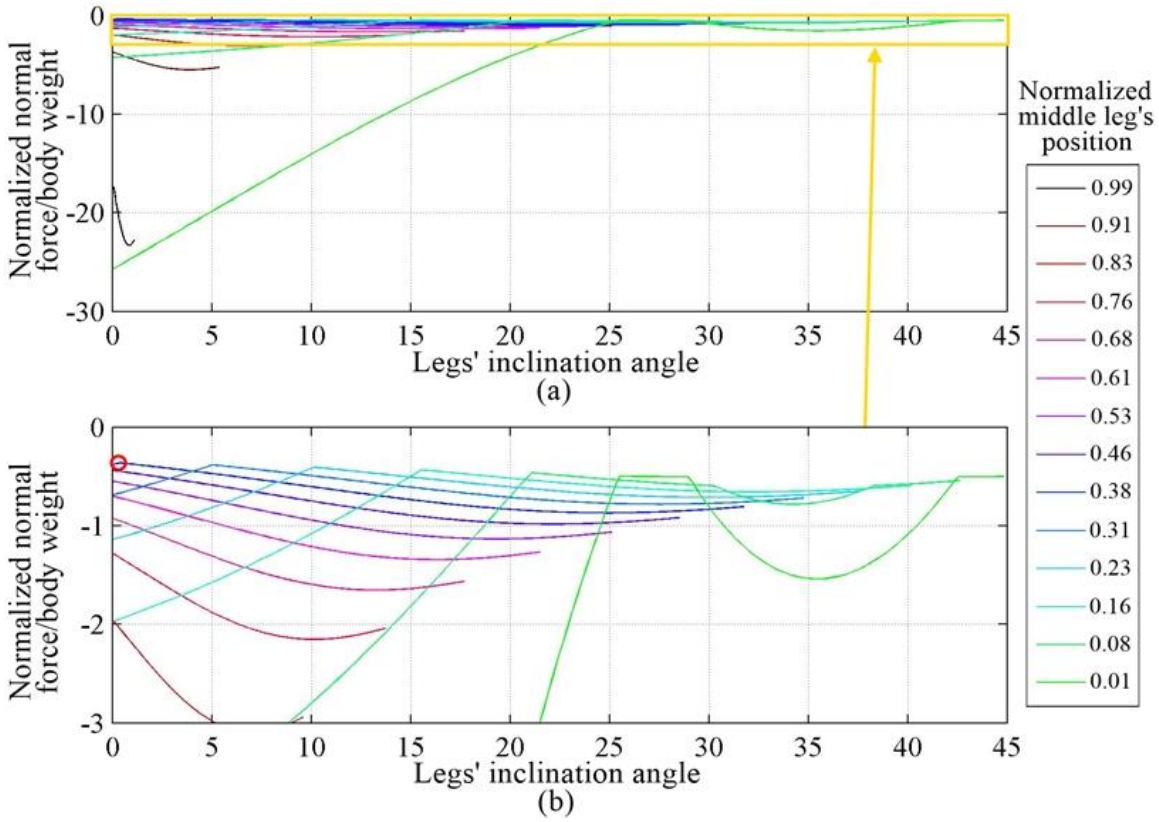

Figure 5.13. (a) The maximum adhesion required by the robot at different legs' inclinations and different middle leg's position. (b) zoomed in view of (a). The red circle in (b) shows the farthest middle leg's position to the hind leg that improves with backward inclination of the middle leg.

An optimization using Genetic Algorithms (GA) is carried out to find the optimal configuration for the structure. It is assumed that the distance between the front and hind tips of the legs and the height are kept fixed at 200 and 100 respectively, and the variables are the position of the middle leg d_h and the inclination of all of the legs, assuming the angles of the legs are given by Equations (5.2) and (5.3), and the range of θ_{inc} is from 0^o to 45^o

$$\min_{d_m,\theta_{inc}} \max\left(F_{yh}, F_{ym}, F_{yf}\right) \quad (5.4)$$

The optimal configuration found is when the inclination of the front and the middle legs is at the maximum front, at -45^o, and the hind leg is at the maximum from the

perpendicular, at -135^o. This result is similar to that found by Yasong et al [18] with the assumption that the structure has infinite stiffness.

5.6. Optimal Robotic Structure

An infinite number of configurations of the robot can be identified when different inclinations of both the body and the legs are considered. The space of the optimal configurations can be summarized in Figure 5.14. For the sake of clarity, this figure shows optimal curves when all the legs have the same absolute value of inclination, and a body inclination range between -30^o and 30^o. In Figure 5.14-a, the front and the middle leg points forward whereas the hind leg points backward. In Figure 5.14-b, the front leg points forward whereas the middle and hind legs point backward. Points on each curve of these figures represent equally optimal configurations from the perspective of minimizing the needed maximum adhesion for the robot to stay on a vertical surface. It should be noted that the maximum required adhesion decreases as the middle leg is positioned closer to the front leg; in fact, the optimal configuration is the one that has the middle leg aligned with the front leg. In Figure 5.14, points on the green curve at the normalized position 0.99 therefore yield the smaller maximum adhesion required for the robot to adhere to vertical surface than any other point presented in this figure.

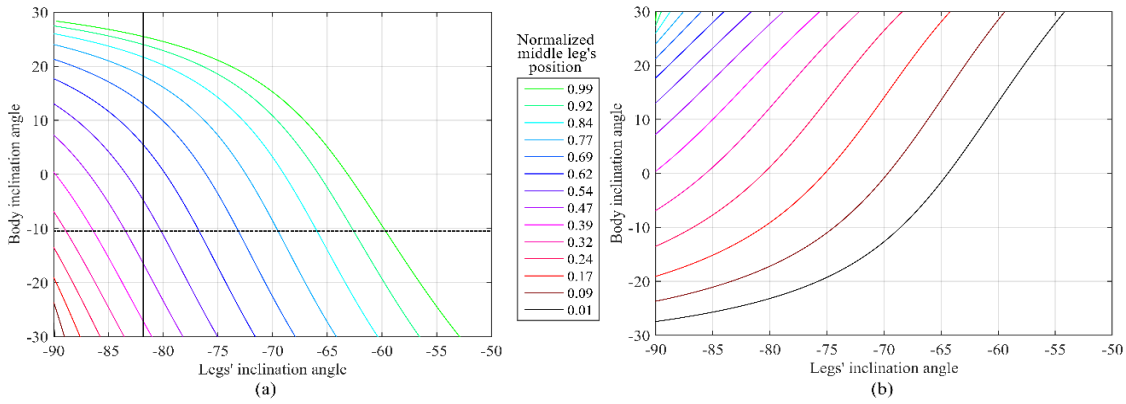

Figure 5.14. Optimal body-legs inclination curves for a number of middle legs positions when (a) the middle leg is inclined forward, (b) the middle leg is inclined backward.

A few optimal configurations chosen from Figure 5.14, for different positions of the middle leg and different body and leg inclinations, are shown in Figure 5.15. Specifically, Figure 5.15-a shows five different optimal configurations when the inclination of the legs was kept constant (configurations shown in Figure 5.15-a were obtained by intersecting the curves of Figure 5.14-a with the vertical black solid line shown in this latter figure). Figure 5.15-b shows five different optimal configurations when the body inclination was kept constant (configurations shown in Figure 5.15-b were obtained by intersecting the curves of Figure 5.14-a with the horizontal dashed black line shown in this latter figure). Figure 5.15-c shows five different optimal configurations when the distance between the tips of the legs on the vertical surface was kept constant (configurations shown in Figure 5.15-c were obtained by intersecting the blue curve of Figure 5.14-a with middle leg's position of 0.69 – see legend of Figure 5.14-a).

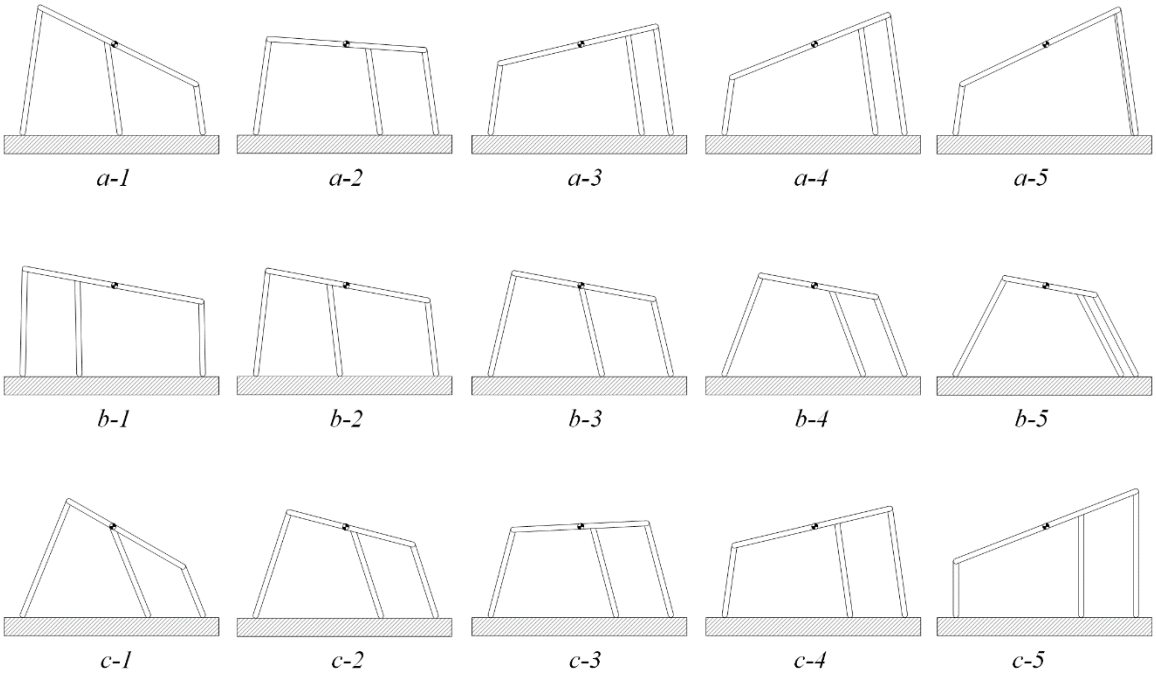

Figure 5.15. Shows few optimal configurations. Subplots a-1 to a-5 are different optimal configurations along the vertical solid black line of Figure 5.14-a when legs are inclined at -82º. Subplots b-1 to b-5 are different optimal configurations along the horizontal dashed line of Figure 5.14-a when the body inclination is -10.5º. Subplots c-1 to c-5 are different optimal configurations at middle leg's position of 0.69 in Figure 5.14-a.

In Figure 5.15, the optimal robotic configurations that have larger middle leg position values use less normal adhesion forces than those with lower middle leg position values. Structures that have the same middle leg position require the same normal adhesion forces although they have different body and legs inclinations.

5.7. Equivalent Leg Design

The robots considered in the previous sections assume that each leg is made up of one single straight beam. However, multi-beam legs are necessary to allow smooth movement for legged robots. In this section, the one-beam leg, see Figure 5.16-a, is replaced with multi-beams leg, see Figure 5.16-b, that allow the robots to use the optimal normal adhesion force on the tips of the legs. The main idea in this section is to change the characteristics of one or more legs to allow the use of optimal normal adhesion for a specific configuration. The one-beam legs of a robotic structure, obtained from the previous section, are used to show the validity of replacing them with multi-beam legs. For the sake of simplicity, only two-beam legs equivalent to the single beam legs are considered, see Figure 5.16.

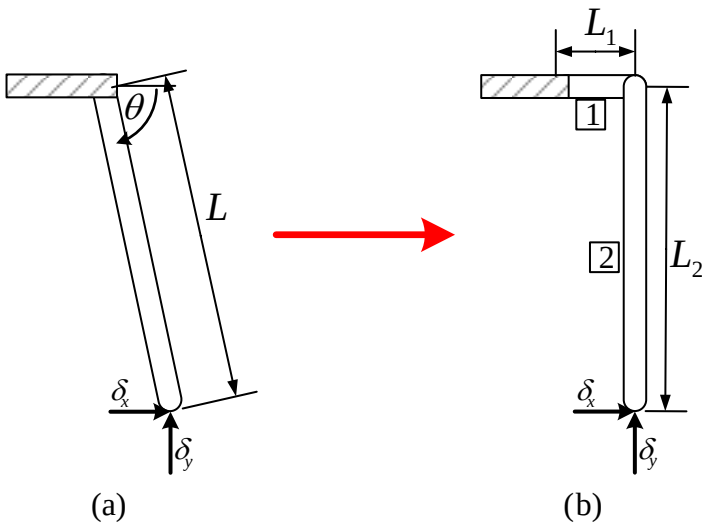

Figure 5.16. (a) one-beam leg. (b) two-beams leg.

The following parameters could be used to find two-beams leg designs equivalent to the one-beam legs:

- The geometry of the legs.
- The stiffness of the legs.
- The cross sectional area.
- The second moment of inertia.
- The thickness of the legs.

An optimal robotic model, randomly chosen from Figure 5.14-a and shown in solid white color in Figure 5.17-a, is used to demonstrate finding two-ink legs equivalent to the single-beam legs. The height to length ratio of the structure is 100:200. The tip of the middle leg is assumed to be positioned at 0.77 of the overall distance between the hind and front legs. The beams of the structure are assumed to have a circular cross-sectional area with a radius of 1. Any three-legged robotic structure requires six angles to define the design of its three two-beam legs, i.e. two angles per leg. Here, it is assumed that the front and the middle legs have the same leg design, i.e. $a_2 = a_3$ and $b_2 = b_3$ in Figure 5.17-a, because they originally had the same length and inclination. The values of a_1 and a_2 are considered as fixed, which reduces the number of the variables to two (b_1 and b_2). The problem is found to be redundant, as there is an infinite number of solutions for this problem if the two variables, (a_1 and a_2), are optimized. Because of that, Genetic Algorithms are used to find the angles of a_2 for a range of a_1 angle values using the following fitness function:

$$\Upsilon = \min_{a_2}(\max(A_{dh})) \qquad (5.5)$$

where A_{dh} is the normal adhesion on the tips of the legs of the robot.

The solution when both a_1 and a_2 are equal to 30^o is shown in Figure 5.17-b. The solution is color-coded, i.e. each leg's configuration with the same color is one solution. In other words, the solution for every inclination angle b_1 of beam B_1 is the angles b_2 and b_3 of beams B_2 and B_3, drawn with the same color. Alternately, Figure 5.17-c shows the different solutions when the values of a_1 and a_2 are 20^o and 40^o respectively.

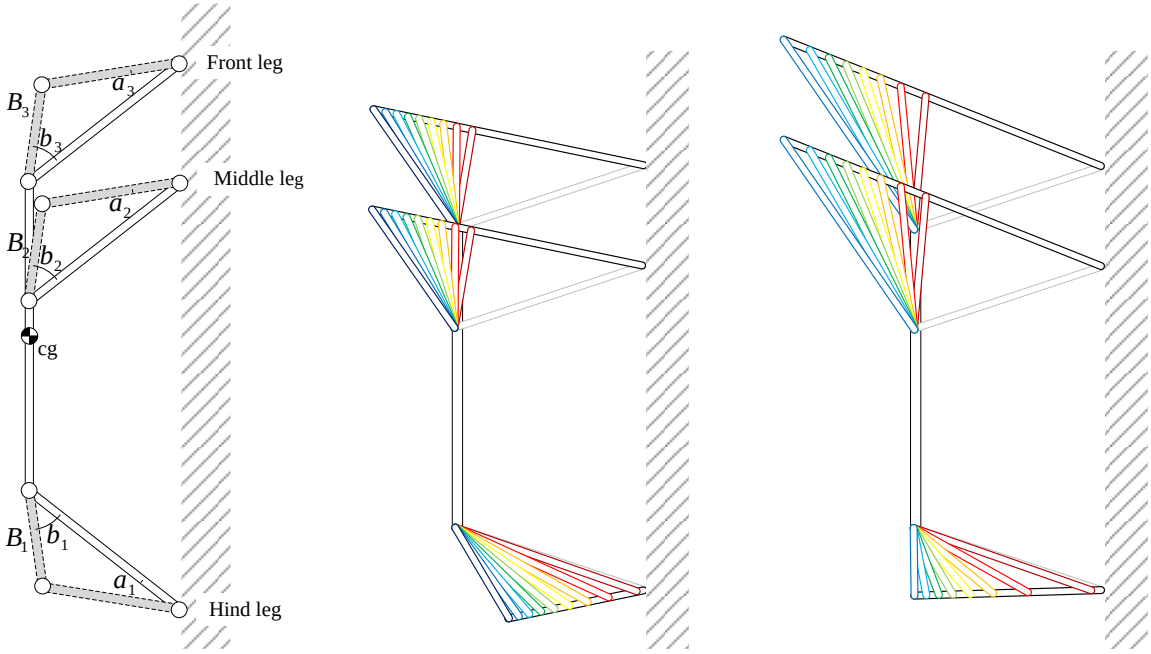

(a) (b) (c)

Figure 5.17. (a) Shows the robotic structure with the corresponding two-beams legs. (b) Shows few possible solutions of having two-beams legs when $a_1 = a_2 = a_3 = 30^o$. (c) Shows few possible solutions of having two-beams legs when $a_1 = 20$, $a_2 = a_3 = 40^o$.

The investigation of the other four parameters is done using the same structure shown in Figure 5.17-a; for the sake of simplicity, the three legs are considered to have two-beams, right angled legs structures. Genetic Algorithms are used to change the investigated parameter of only the front leg in order for the robot to use the optimal normal adhesion force. The parameters are investigated for only one leg as it is the smallest number of legs that needs to be changed in order to minimize the maximum normal adhesion and produces a single solution.

Table 5.1 summarizes the results of changing the four parameters independently; the shaded cells highlight the investigated parameter in each row. The first row shows the values of the parameters before the optimization. In which the maximum adhesion is not the optimum, as the legs of the structure are constructed using right angled two-beam legs. The shaded cell in Row 2 shows the optimal stiffness of the leg that

produces the optimal normal adhesion force. The stiffness of the leg is presented as a fraction of the stiffness of the beams constructing the rest of the structure. The parameters used for the optimization in the third and the fourth rows are the cross sectional area and the second moment of inertia, respectively. In the last row, the thickness of the front leg is optimized. The optimal radius value of the front leg is found to be 1.248. The fifth row shows a change in both the cross sectional area and the second moment of inertia. Both parameters are varied because, a change in the thickness of the leg, assuming the beams have circular cross section, will change both values of the cross sectional area and the second moment of inertia. The validity of the optimal values is done by calculating the normal adhesion force using ANSYS. In fact, the maximum error, amongst the five cases, is found to be 0.03% of the maximum adhesion value.

Table 5.1. Investigated parameters for front leg design

Row #	Optimized parameter	stiffness	Cross sectional area	Second moment of inertia	Max. adhesion	Max. Adhesion (ANSYS)
1	None	1	3.14	0.78	0.54	0.54
2	Stiffness	0.41	3.14	0.78	0.28	0.28
3	Cross sectional area	1	8.25×10^{-4}	0.78	0.28	0.28
4	Second moment of inertia	1	3.14	0.32	0.28	0.28
5	Radius	1	2.01	0.32	0.28	0.28

5.8. Discussion

The effect of the different geometric parameters on the normal adhesion force requirements on robots with finite stiffness materials is investigated. However, only the height to length ratio and the middle leg's position are investigated for robots with infinite stiffness materials. Only the position of the tips of the legs are considered without taking into account the shape of the legs.

In the case of 90^o inclination legs, i.e. perpendicular to the climbing surface, the best position for the middle leg is when it is positioned approximately close to 0.32. The

maximum adhesion increases as the middle leg's position gets closer to the front leg. in fact, the maximum is when the middle leg is very close to the front around 0.98 of the distance between the hind and the front legs. However, the maximum adhesion decreases as the middle leg gets closer to the front leg as long as the body or the legs inclination angle changes to minimize the adhesion. The high adhesion in case of legs inclined at 90^o is a result of the moment at node 3, in Figure 4.2, which induces tension in the front leg and compression in the middle leg, see Appendix B. The moment in node 3 when inclining the body and the legs has less effect than that in the perpendicular case. Because, the effect of the moment is distributed along longer beams, which resulted from the inclination of the legs or the body. The Maximum adhesion found in Figure 5.8 and Figure 5.11 matches with that in Figure 5.3 for any middle leg position. Provide the use of the optimal inclination angle for each middle leg position. It could be concluded from this is that, if the front leg has higher adhesion than that of the middle leg's, then the body, the legs or both should be inclined to distribute the adhesion amongst the front and the middle legs.

In case of infinite stiffness structures, the optimal maximum normal adhesion force requirement decrease as the middle leg is positioned close to the front leg. While, the maximum normal adhesion force dramatically increases when the middle leg gets close to the front leg for structures with finite stiffness materials. The high normal adhesion force is due to the stresses in the structures. The effect of the stress could be decreased by using more flexible legs, one way is by using thinner legs. Figure 5.5 shows that using small radius legs, close to 10^{-2}, permits using low adhesion forces on the tips of the legs for middle legs positions very close to the front.

The effect of changing the geometrical parameters on the normal adhesion force requirement is summarized in the Table 5.2. The first column is for structures with torque controlled motors, the second column is for structures with position controlled legs and perpendicular legs, and the third column is for structures with position controlled legs and inclined legs and body. Note that the leg and body inclinations do not affect the normal adhesion force for infinite stiffness structures. This is because such structures depend only on the position of the tips of the legs with respect to the CoM and not on the shape of the structure.

Table 5.2. The effect of changing the different geometrical parameters on the normal adhesion force

Property	Infinite stiffness structures	Finite stiffness structures (perpendicular legs)	Finite stiffness structures (inclined legs and body)
Lowering the height	Normal adhesion reduces	Normal adhesion reduces	Normal adhesion reduces
Increasing the body length	Normal adhesion reduces	Normal adhesion reduces	Normal adhesion reduces
Increasing the normalized middle leg position	Normal adhesion reduces	As the position goes away from 0.3 position, the normal adhesion increases	Normal adhesion reduces
Legs inclination	No influence	Not applicable	See Figure 5.14
Body inclination	No influence	Not applicable	See Figure 5.14

The presented results yield the following guidelines to design an optimal robot structure, which minimizes the maximum adhesion on the tips of the legs, with a 1:2 height to length aspect ratio, loitering on a vertical surface:

1. For a fixed body length, all the legs of the robot should incline outwards, and extend as far as possible to increase the distance between the front and the hind tips of the legs.
2. The position of the tip of the middle leg should be as close as possible to the front leg and the inclination should be forward for a middle leg's position between approximately 0.4 to 1, and backward otherwise.
3. The best middle leg's tip position is found when the middle leg's tip position is at the same position as the front leg's; this finding is confirmed through an optimization performed using GA, see Equation (5.3).
4. Depending on the height to length ratio, tilting the body mostly improves the adhesion requirement for the robot.
5. The optimal body and legs inclination for any middle leg's position could be chosen from Figure 5.14.

6. Finding a proper leg design by either finding optimal geometric legs or by using any desired geometry and then tune the design by changing one of the variables in Table 5.1.

Points 1 to 4 is applicable to any robot with any height to length aspect ratio. While points 5 and 6 are required to be recomputed for the robot with the desired height to length ratio.

It is shown that the thickness of the body of the robot should be maximized and the one of the legs minimized. Since the analysis was performed by considering a constant mass of the robot, the above-mentioned result implies that the stiffness of the body of the robot should be higher than that of the legs.

An interesting remark is that by decreasing the stiffness of the legs, a better approximation introduced by connecting the legs to the vertical wall via hinges is obtained.

Similar to the model used in Chapter 3, the FEM model used here considers the worst case scenario in terms of weight distribution. It assumes the weight to be concentrated at the center of mass of the body, rather than being distributed on the legs of the robot which brings the CoM closer to the vertical surface. Moreover, the shape of the feet is simplified to be one point per leg similar to Chapter 3.

Chapter 6.

Assess if the FEM Analysis of the Robot is Viable

6.1. Introduction

To verify our assumptions and calculations, the simplified developed model, in the previous chapter, is used to investigate the stance of the ants when loitering on vertical surfaces. Ants are chosen for this study because they are good climbers and they also have a configuration similar to the studied six-legged robot [87].

6.2. Ants Model Simplification

The ant along with the equivalent robot structure, highlighted in yellow, are shown in Figure 6.1-a. The legs are simplified to be consistent of one beam, as the ant is in state of no-motion, and one hinge at the connection with the surface to simulate the (tarsus and pre-tarsus) of the ant's leg. The measured parameters used to simplify the structure of the ants to match the robot's are shown in Figure 6.1-a and Figure 6.1-b, where:

T_B is the distance between the front and hind legs' tips.

S_B and T_{cm} are the body's length and position respectively.

S_h is the position of the middle leg's coxa.

T_h is the position of the middle leg's tip.

h is the height.

r, not shown in Figure 6.1, is the body and legs' thickness.

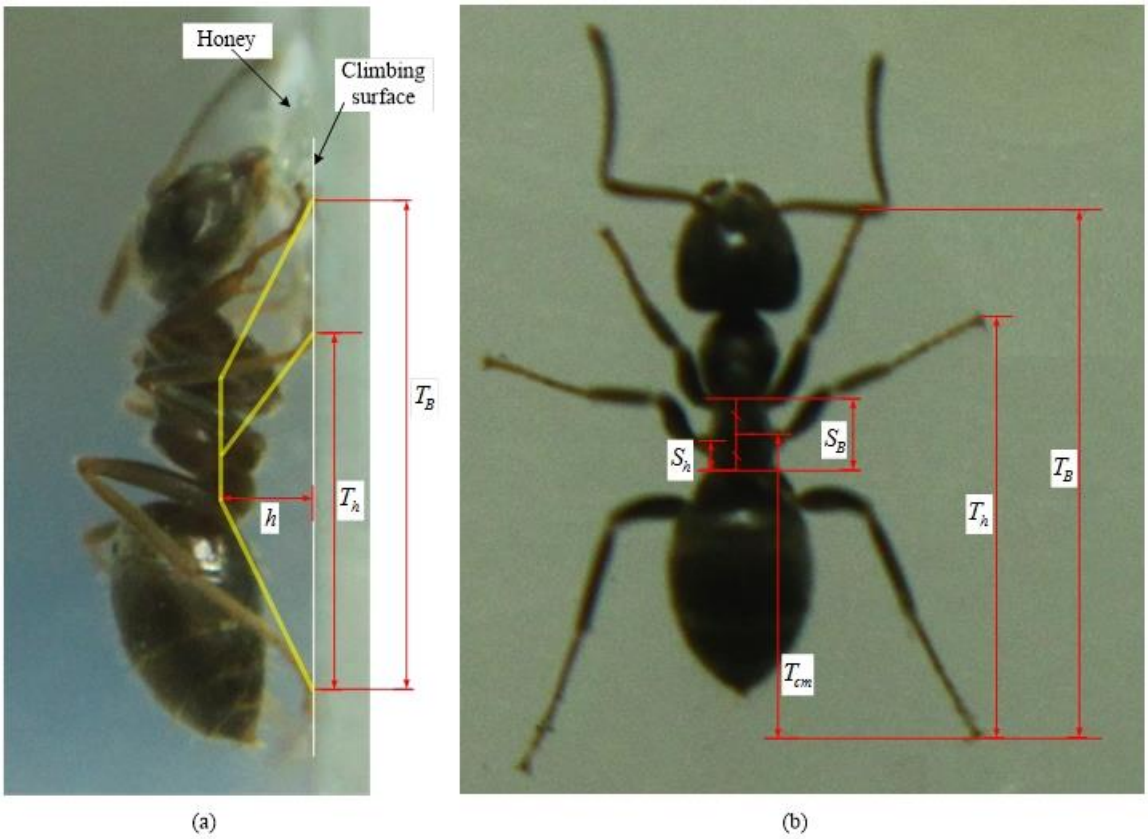

Figure 6.1. Shows the parameters measured from the ants, (a) Lateral view, (b) Dorsal view.

The length of the body S_B is measured as the distance between the front and the hind legs' first segments, called coxas, see Figure 6.2. The position of the body T_{cm} is measured as the distance from the center of the body's length to the hind leg's tip. The measurement of the middle leg's coxa position S_h is represented as the distance between the coxa of the hind leg and the coxa of the middle leg. When the ratio equals 0, then the middle leg's coxa is at the same position as the hind leg's coxa. The position of the coxa approaches the front leg's coxa as the value of S_h approaches 1.

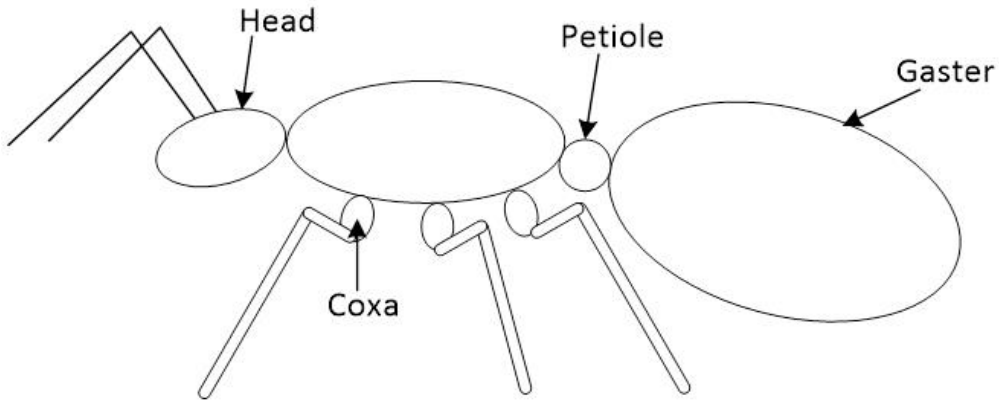

Figure 6.2. The different parts of ant.

6.3. Carried Experiment

The ants are photographed when they are standing still to feed off honey drops on a surface of vertical surface. A small model, made of plexi-glass, that has a square cross section is built to facilitate photographing the ants from different orientations, see Figure 6.3. The base of the model was designed to be bigger than the top, to make it easier to put the model over the ant(s) without harming them. A cap is used to close the top of the structure to facilitate cleaning and allowing the ants to exit; moreover, the cap has holes to allow the ants to breathe. In total 150 ants are used, where 91 ants are photographed from either the top or the bottom, similar to that shown in Figure 6.1-b, and 59 ants are photographed from the side, similar to that shown in Figure 6.1-a.

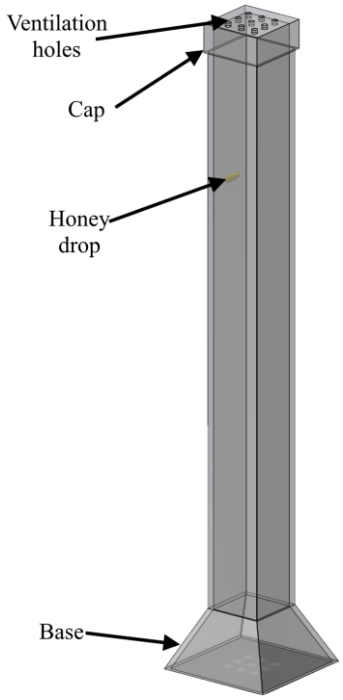

Figure 6.3. A CAD model for the setup used to photograph the ants.

In both of the photographed positions, i.e. from above and the side, the following parameters are measured:T_B, S_B, T_{cm}, S_h ,and T_h (see Figure 6.1). The height is measured only using the photos captured from the side. The photos captured from above are used to make sure that the ants are standing up vertically with an angle range of $\pm 20^{o}$ from vertical, since a change in the orientation of 20^{o} would decrease the force pulling an ant to the back, due to gravity, by only $\pm$6%.

The position of the middle leg's tip T_h is the distance between the front and the hind legs' tips. The height of the robot h is presented as the distance from the petiole to the climbing surface, which is considered the point of force application. The Petiole is chosen because it is the point by which the gaster (which has a large weight ratio) is attached to the body, see Figure 6.2. The average thickness of the legs r is measured graphically. Specifically, the thickness of each segment of the leg is averaged over the length of the leg. The thickness is calculated using the following equation:

$$Thickness = \frac{\sum_{i=1}^{n}(segment\ thickness \cdot length\ of\ that\ segment)}{length\ of\ the\ leg} \quad (6.1)$$

where n is the number of segments in the leg.

All of the measurement data is presented as ratios to overcome the variation in ants' sizes. T_B is considered as a measuring unit for all of the measurements, i.e. $T_B = 1$, except for S_h which is measured with S_B as the measuring unit.

Assuming a robot with $T_B = 200$, which has the same T_B as the robots investigated earlier, the parameters of the robot equivalent to the ants' geometry are calculated and shown in Table 6.1. The weight of the ant is considered to be a unit to facilitate the representation of the force to be a fraction of the overall weight.

Table 6.1. Parameters measured experimentally and the equivalent values used in calculations.

Parameter	Experimentally	Value
T_B	1	200
T_h	0.62	124
h	0.1439	28.78
S_B	0.169	33.8
S_h	0.358	12.1
T_{cm}	0.616	123.25
r	0.022	4.4

6.4. Ants' Middle Leg's Position

The developed mathematical model presented earlier is used to compute the maximum required adhesion force for S_h and T_h while keeping all the other parameters fixed. The value of S_h is varied within the full range of 0 to 1, with the middle leg's coxa coinciding with the hind leg's coxa when $S_h = 0$, and coinciding with the front leg's coxa

when $S_h = 1$. Similarly, the value of the middle leg's tip position T_h is considered to be 0 when the tip is aligned with the hind leg's tip, and 1 when the middle leg's tip is aligned with the front leg's tip, i.e. the distance to the hind leg's tip is 200.

The maximum required adhesion at different values of T_h and S_h for a unit force representing the weight at the center of mass is shown in Figure 6.4. It is noted that the smaller the distance between the middle and hind legs' coxas is, the less the maximum required adhesion force is. From the photos of the ants, the middle and the hind legs' coxas are as close as possible to each other; in fact, the mid and the hind coxas are in contact with each other. The ratio of the distance between the center of the middle leg's coxa and the center of the hind leg's coxa to the distance between the centers of the hind and the front coxas is 0.358.

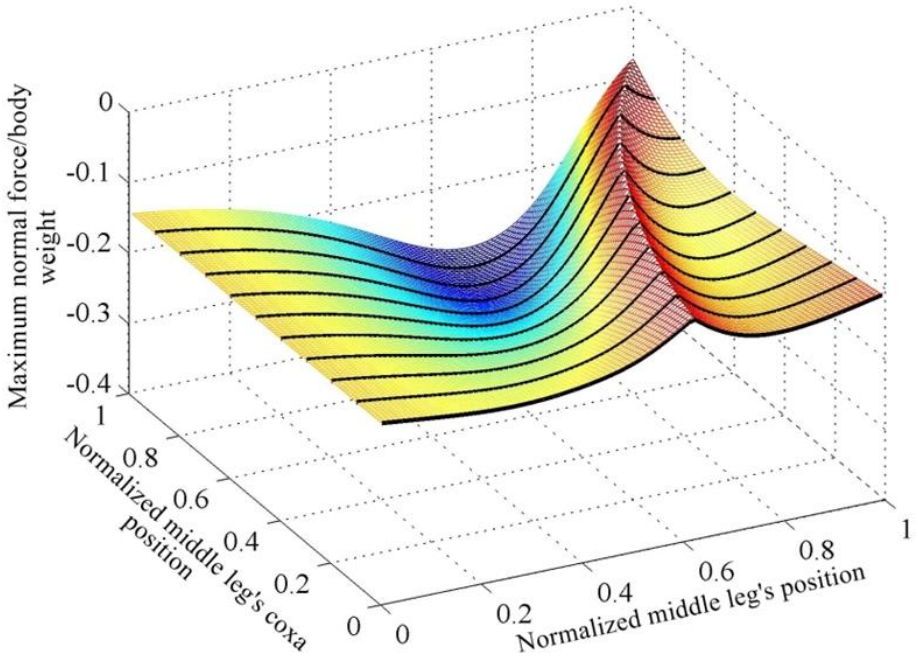

Figure 6.4. Shows the adhesion requirement for different middle leg's coxa and tips positions.

Figure 6.5 shows the maximum normalized adhesion force when a ratio between S_B and S_h of 0.36 is considered. The different lines in this figure represent forces for the different heights the ants had in the recorded images. The black line in Figure 6.5 shows the force for the median height of the ants. The position of the middle leg's tip used by

the ants is plotted as a solid red line, with its standard deviation plotted as a red dashed line. The optimal position for the tip is at 0.69, which corresponds to the highest point on the black curve marked with yellow circle in Figure 6.5, is not far from that found experimentally with the ants. In fact, the ants' average position of the middle leg's tip is different by only 8% away from the calculated optimal tip position.

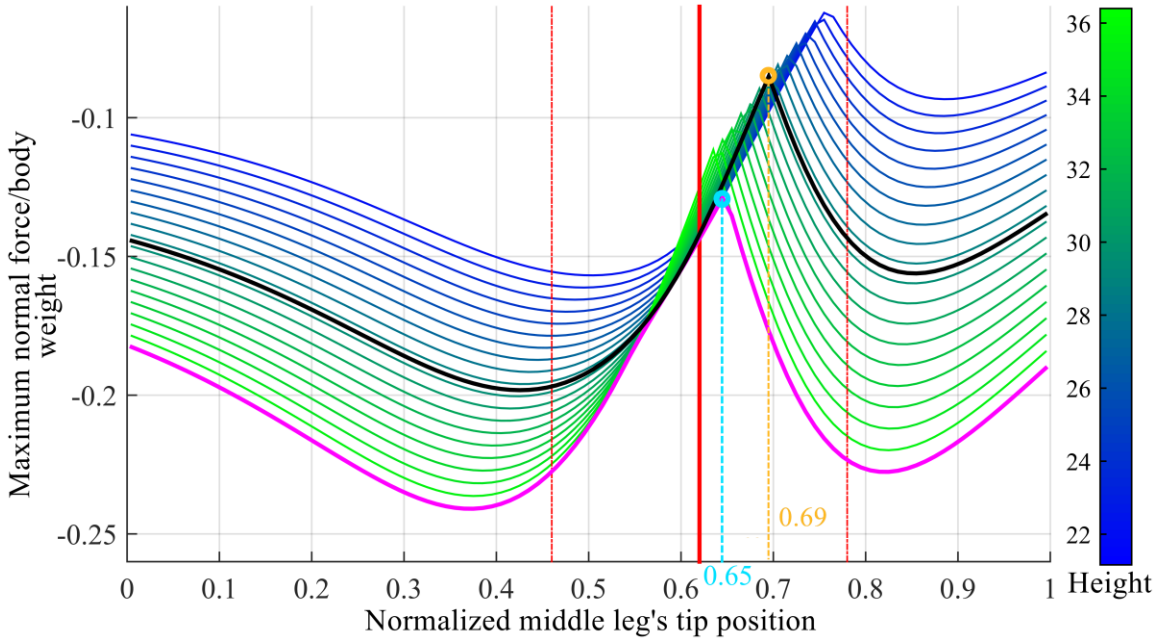

Figure 6.5. The normal force requirement at different heights, in colors varies from green to blue. The black line is the normal force requirement at the median height, the middle leg's tip position obtained experimentally is shown in solid red line and its standard deviation in dashed red lines.

Curves of maximum normal force for a range of heights for the robot are shown in Figure 6.5, colored with shades varying from blue to green; the different heights are added to the figure to analyze the effect of changing the height, because the authors noticed that the ants change their body height while loitering. The magenta line in Figure 6.5 is obtained by intersecting all the curves in this figure and considering their lower values for each middle leg's tip position. It therefore represents the maximum normal adhesion requirement for each position of the middle leg's tip at different heights. It should be noted that the maximum value of this line is close to the averaged middle leg position of the ants (vertical red line in Figure 6.5). The maximum point on that curve, marked with a cyan circle, represents the position of the middle leg's tip that experiences

the minimum adhesion force requirement for the different heights theoretically. That point is different by only 6% from the middle leg position used by the ants experimentally.

The thickness of the body used in the calculations is approximated to be 5 times the thickness of the legs. The effect of body thickness on the curve of the maximum adhesion and the position of the minimum adhesion point is shown in Figure 6.6. Although the curves are not identical between the considered thicknesses, the point that requires the minimum adhesion is still the same for the different radius values.

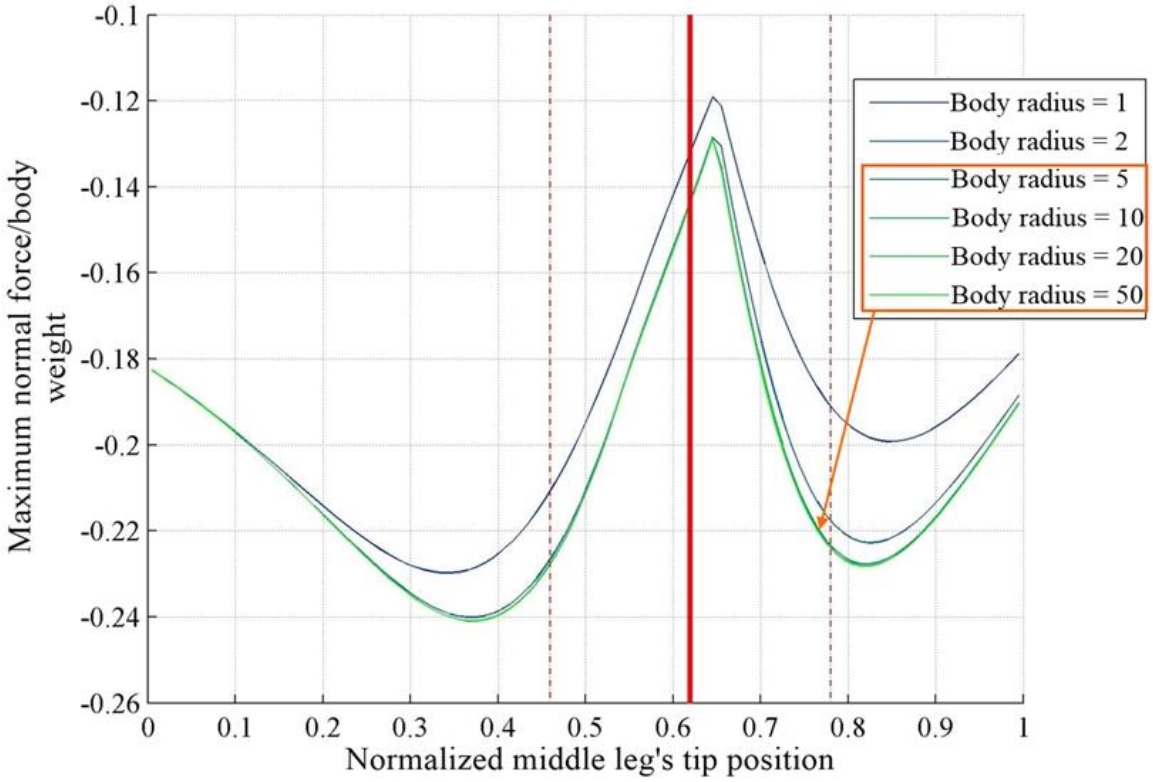

Figure 6.6. Shows the maximum normal force requirement for different body thicknesses at different middle leg's position. The considered body thicknesses are 1, 2, 5, 10, 20 and 50 times the thickness of the legs, they are highlighted in gradient colors from blue to green. The body thicknesses of 5 and higher overlap. The solid red line is the middle leg's tip position obtained experimentally and the dashed red lines are the standard deviation.

6.5. Discussion

The steps used to investigate the effect of the different parameters on the structure of the robot are used to analyze the stance the ants use on vertical surfaces. Analytically, it is found that the closer the middle leg's coxa is to the hind leg's coxa the less the adhesion force is over the entire range of the middle leg's tip position. Interestingly, the coxas of the middle and the hind legs are touching each other in ants, that is they are as close as their size allow. The distance from the center of the coxa of the middle leg to the center of the coxa of the hind leg is 33% of the body length on average on the collected ants. The optimal middle leg's tip position is at approximately 61% of the distance between the tips of the hind and front legs pointing forward. It could be concluded, from Figure 6.5, that the ants position their legs at approximately 0.61 to optimize the adhesion force requirement while they are loitering on vertical surfaces.

Chapter 7.

Maximum Torque Minimization as Secondary Objective

7.1. Introduction

This chapter presents minimizing the maximum torque on the joints of climbing robots, with force/torque controlled legs, while keeping the maximum normal adhesion force at minimum. That is possible because, the description of the system, given by Equations (3.1) to (3.3) presented in Chapter 3, has 6 variables; moreover, it also has one constraint equation, i.e. Equation (3.8), which combined produces a system with two degrees of freedom. This optimization is important because, it can be utilized to use weaker and smaller motors help decrease the mass of the robot and in turn the adhesion requirements, see Equation (3.8); using weaker motors helps decreases the cost of building the robot, as weaker motors are mostly cheaper than the stronger ones. Deriving the joints using low torque is equivalent to using low current which helps in increasing the life cycle of the motors. In this chapter, the maximum torque on the joints of the robot is minimized, without compromising the optimal adhesion requirements on the tips of the legs, while climbing a vertical surface [89].

7.2. Minimizing the Maximum Torque

Minimizing the maximum torque for a robotic structure is a problem that is non-linear, and non-differentiable which could be solved by a non-linear optimizer such as the Genetic Algorithms. However, the problem could be transformed to a linear quadratic form and solved faster and more accurately than using other optimizers. Transforming

the non-linear problem into linear is presented first and a comparison with other three widely used optimizers is presented second.

7.2.1. Robotic Model

The legged robot investigated in this work is assumed to be a three legged, 2-dimensional simplified version of a six legged robot, similar to that of ants. The robot is assumed to have identical right and the left halves, which is the reason for the simplification. Figure 7.1 shows the robot with a rigid structure and three legs attached to a vertical surface. Each leg has two revolute joints, equipped with revolute motors. The six motors exert torque on the six joints to keep the robot in position and to withstand the force of gravity (gravity is pointing to the negative x-axis in Figure 7.1).

The identification of the set of the torques that minimize the maximum torque applied by each motor is generally desired in order to minimize the torque requirements of the motors. By reducing the torque requirements, the size of the motors to be selected decreases, and in turn the mass of the robot decreases. Minimizing the mass of climbing robots is relevant in order to increase their climbing performance [18].

The relationship between the forces on the tips and the torques applied by the joints is calculated using the Jacobian [90], which, for a two-link mechanism, is given by:

$$\begin{bmatrix}\tau_{i1}\\ \tau_{i2}\end{bmatrix} = J_i^T \cdot \begin{bmatrix}f_{ix}\\ f_{iy}\end{bmatrix} \tag{8.1}$$

$$J_i = \begin{bmatrix}-d_2 \cdot s_{i1,i2} - d_1 \cdot s_{i1} & -d_2 \cdot s_{i1,i2}\\ d_2 \cdot c_{i1,i2} + d_1 \cdot c_{i1} & d_2 \cdot c_{i1,i2}\end{bmatrix} \tag{8.2}$$

where τ_{i1}, τ_{i2} are the torques in leg i for the first, the closer to the body, and the second, the further away from the body, joints respectively; f_{ix} is the x-axis force component at the tip of leg i; f_{iy} is the y-axis force component at the tip of leg i; J_i is the Jacobian for leg i; d_1, d_2 are the length of the first and the second links of leg i; s_{i1} is the sine of the angle of the first joint in the i^{th} leg, $s_{i1\,i2}$ is the sine of the sum of the first and the

second angles of the i^{th} leg; c_{i1} is the cosine of the angle of the first joint of the i^{th} leg and $c_{i1,i2}$ is the sine of the sum of the first and the second angles of the i^{th} leg.

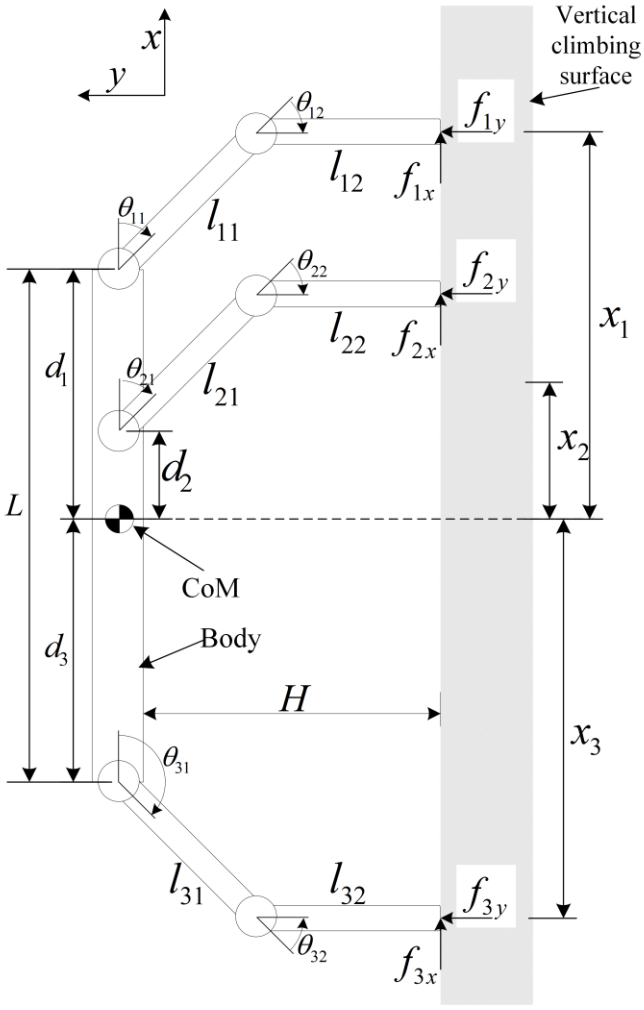

Figure 7.1. Three-legged robot climbing a vertical wall.

The torque equations for the robotic structure are:

$$\tau_{11} = \left|\left(-l_{12} \cdot s_{11,12} - l_{11} \cdot s_{11}\right) \cdot F_{1x} + \left(l_{12} \cdot c_{11,12} + l_{11} \cdot c_{11}\right) \cdot F_{1y}\right| \quad (8.3)$$

$$\tau_{12} = \left|\left(-l_{12} \cdot s_{11,12}\right) \cdot F_{1x} + \left(l_{12} \cdot c_{11,12}\right) \cdot F_{1y}\right| \quad (8.4)$$

$$\tau_{21} = \left|\left(-l_{22} \cdot s_{21,22} - l_{21} \cdot s_{21}\right) \cdot F_{2x} + \left(l_{22} \cdot c_{21,22} + l_{21} \cdot c_{21}\right) \cdot F_{2y}\right| \quad (8.5)$$

$$\tau_{22} = \left|\left(-l_{22} \cdot s_{21,22}\right) \cdot F_{2x} + \left(l_{22} \cdot c_{21,22}\right) \cdot F_{2y}\right| \tag{8.6}$$

$$\tau_{31} = \left|\left(-l_{32} \cdot s_{31,32} - l_{31} \cdot s_{31}\right) \cdot F_{3x} + \left(l_{32} \cdot c_{31,32} + l_{31} \cdot c_{31}\right) \cdot F_{3y}\right| \tag{8.7}$$

$$\tau_{32} = \left|\left(-l_{32} \cdot s_{31,32}\right) \cdot F_{3x} + \left(l_{32} \cdot c_{31,32}\right) \cdot F_{3y}\right| \tag{8.8}$$

where l_{i1}, l_{i2} are the lengths of the links of the leg i for the first link, the closest to the body, and the second, the furthest away from the body.

In a static case, the following equilibrium of the forces and torques must be met:

$$\sum F_X = f_{x1} + f_{x2} + f_{x3} - m \cdot g = 0 \tag{8.9}$$

$$\sum F_Y = f_{y1} + f_{y2} + f_{y3} = 0 \tag{8.10}$$

$$\sum M_Z = H \cdot f_{x1} + H \cdot f_{x2} + H \cdot f_{x3} - x_1 \cdot f_{y1} - x_2 \cdot f_{y2} - x_3 \cdot f_{y3} = 0 \tag{8.11}$$

where F_x and F_y are the forces acting along the x-axis and the y-axis on the robot's center of gravity, m is the mass of the robot, g is the gravitational acceleration, H is the height of the robot and x_1, x_2 and x_3 are the x-axis coordinates of legs 1, 2 and 3 respectively, d_1, d_2 and d_3 are the distance between legs 1, 2 and 3 respectively to the center of mass along the body of the robot.

7.2.2. Problem Definition

The investigated problem can be defined as finding the minimum of the maximum of m number of absolute value equations in n variables, which can be written as follows:

$$\psi(x) = \min_{\mathrm{x}}(\phi(x)), \quad x \in \mathbb{R}^n \tag{8.12}$$

where

$$\phi(x) = \max\left(f_1(x), \ldots, f_m(x)\right) \tag{8.13}$$

where each of the objective functions $f_i(x)$ is an absolute value linear function:

$$f_i(x) = |g_i(x)| \tag{8.14}$$

where , $i = 1, \dots, m, \quad g_i: \mathbb{R}^n \to \mathbb{R}$

Equation (8.14) can be formulated as follows:

$$f_i(x) = \max\big(F_{1i}(x),\ F_{2i}(x)\big) \tag{8.15}$$

where

$$\begin{matrix} F_{1i}(x) = g_i(x) \\ F_{2i}(x) = -g_i(x) \end{matrix}, \quad i = 1, \dots, m \tag{8.16}$$

An example of the functions $f_i(x)$, $F_{1i}(x)$, and $F_{2i}(x)$ for a low dimensional case is shown in Figure 2, with 1 absolute value equation ($m = 1$) in one variable ($n = 1$).

By using the formulation presented by (8.12) – (8.15), the function that gives the maximum of a set of absolute linear functions is:

$$\phi(x) = \max\big(f_1(x), \dots, f_m(x)\big) = \begin{cases} F_1(x) & if \quad F_1(x) \geq \big(F_2(x) \vee \dots \vee F_{2m}(x)\big) \\ \vdots & \vdots \\ F_{2m}(x) & if \quad F_{2m}(x) \geq \big(F_1(x) \vee \dots \vee F_{2m-1}(x)\big) \end{cases} \tag{8.17}$$

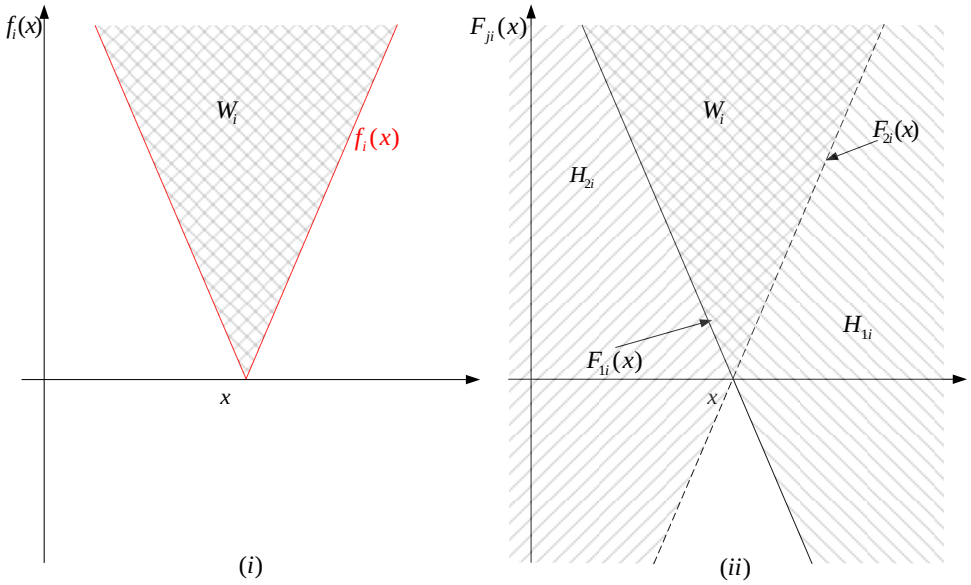

Figure 7.2. Two dimensional example representing the function fi(x) in (i) and the functions F_{1i} and F_{2i} in (ii).

In order to find the function ϕ, we define wedge, W, as the intersection of two upper hyperspaces, where an upper hyperspace H is defined as the space bounded between a hyper-plane and $+\infty$ [91]. The upper hyperspace H can be represented by the following equation:

$$H = \{x \in \mathbb{R}^n | Ax \geq b\} \qquad (8.18)$$

where A is a vector of constant coefficients and b is a constant coefficient. For instance, Figure 7.2 shows the upper hyperspaces H_{1i} and H_{2i} respectively generated by the hyperplanes F_{1i} and F_{2i}, see Equation (8.15). Figure 7.2 also shows the wedge W_i for a low dimensional space, which is generated by the intersections of the hyperspaces H_{1i} and H_{2i}.

For example, in the low dimensional case, Figure 7.3 for instance shows ϕ defined by the intersection of six half-planes $H_{ji},\ j = 1,2,\ i = 1,2,3$ (intersection of 3 wedges $W_i, i = 1,2,3$). The surface ϕ is an open convex shape, shown using solid lines in Figure 7.3, and the solution ψ is shown as a point.

In higher dimensions, the intersection of the wedges form a high dimensional open convex shape represented by ϕ in Equation (8.12). The vertices of the open convex shape can be found by calculating the intersection points generated by the half planes.

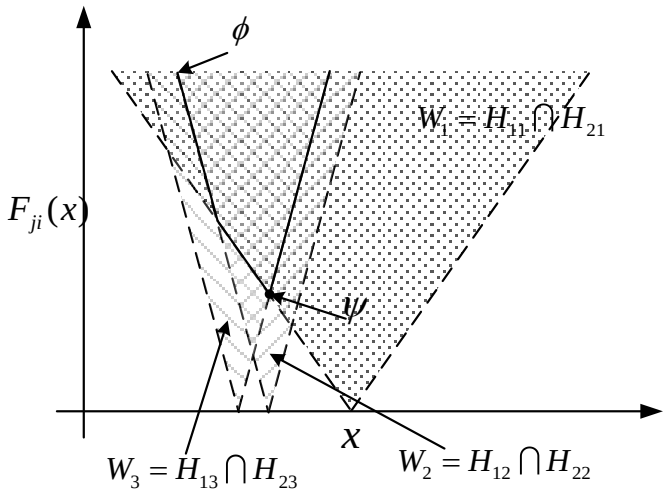

Figure 7.3 ϕ is bounded by solid lines is generated by the intersection of three wedges W_1, W_2 and W_3.

Any intersection point in $(n+1)$ dimensional space (n variables problems), needs at least $(n+1)$ non-parallel hyper-planes. For example, an intersection point in two dimensional space (one variable problem) can be formed using two non-parallel half-planes, and in three dimensional space (two variables problem), three non-parallel half-planes are needed to form an intersection.

The intersection points of $(n+1)$ hyper-planes can be computed by writing the equations to be solved as $\mathbb{A}\boldsymbol{X} = \boldsymbol{B}$, where $\mathbb{A}$ is the matrix containing the vector of constant coefficients $\boldsymbol{A}$, and $\boldsymbol{B}$ is a vector that contains the constant coefficients b for the hyper-planes. The solution can be computed by $\boldsymbol{X} = \mathbb{A}^{-1}\boldsymbol{B}$, which will have a solution only if $\mathbb{A}$ is full rank. If $\mathbb{A}$ is not full rank, the hyper-planes do not intersect in a point, they either intersect in a dimension higher than one point or do not have a common intersection space.

The constraints could also be taken into account, assume the constraints are given as follows:

$$F_c(x) \geq b_c \qquad (8.19)$$

where $F_c(x)$ is the matrix containing the coefficients of the constraints and b_c is the vector of constant coefficients. The intersection points that do not satisfy the constraints would be rejected as they are not valid solutions. In Figure 7.4, the points $\gamma_3, \gamma_4, \gamma_7$ and γ_8, are not a solution because they are not satisfying the constraints. The optimum point in Figure 7.4 is γ_9, since it is the maximum of the minimum that satisfies all of the constraints. The constraints are used as equations to be optimized, i.e. adding them to the $2m$ equations.

The problem is convex in nature. The intersection of the wedges, wedges are convex in nature, is convex. Also the intersection of the convex shape resulted from the intersection of the wedges with the constraints, which are convex, is convex.

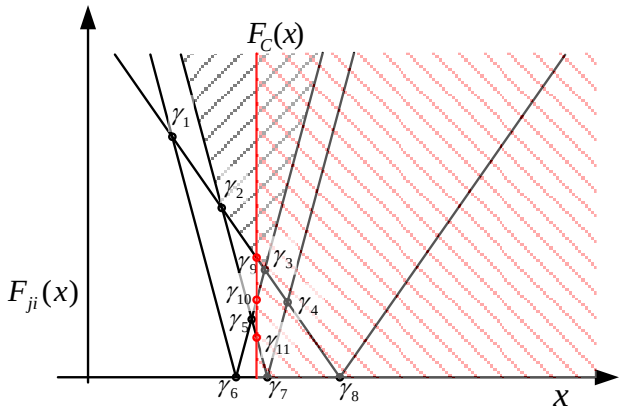

Figure 7.4 Shows absolute linear equations with constraint *$F_c(x)$*

7.2.3. Numerical Example

In order to show the performance of the formulation and linear programming algorithm comparing to other optimizers, arbitrary geometrical parameters of the robot were selected. Specifically, the body of the robot in Figure 7.1 was assumed to be 1m long and the hip joints $\theta_{i1},\ i = 1,2,3$, were assumed to be positioned 0.5m apart. The first segment of each leg, $l_{i1},\ i = 1,2,3$, was 0.5m long and the second segment, $l_{i2},\ i = 1,2,3$, was 0.6m long. The height of the robot was assumed to be 0.9m, and the x-axis positions of the legs 1, 2 and 3 were 0.9m, 0.4m and -0.9m respectively, considering

zero is at the center of gravity. The weight of the robot was assumed to be 500N. The robot is assumed to use adhesive pads to stay attached to the wall, and each pad can withstand a maximum force of 150 N. Which poses the following constraints:

$$F_{iy} \geq -150, \quad i = 1,2,3 \tag{8.20}$$

The mentioned numerical values of the problem's parameters, the torque Equations (8.3) to (8.8) and the equality constraints, Equations (8.9) to (8.11) yield the following equations:

$$\tau_{11} = \left|-0.9 \cdot F_{2x} - 0.9 \cdot F_{3x} + 1.04 \cdot F_{3y} + 90\right| \tag{8.21}$$

$$\tau_{12} = \left|-0.6 \cdot F_{2x} - 0.6 \cdot F_{3x} + 300\right| \tag{8.22}$$

$$\tau_{21} = \left|0.9 \cdot F_{2x} - 1.44 \cdot F_{3y} + 360\right| \tag{8.23}$$

$$\tau_{22} = \left|0.6 \cdot F_{2x}\right| \tag{8.24}$$

$$\tau_{31} = \left|0.9 \cdot F_{3x} - 0.4 \cdot F_{3y}\right| \tag{8.25}$$

$$\tau_{32} = \left|0.6 \cdot F_{3x}\right| \tag{8.26}$$

subject to the following inequality constraints:

$$F_{3y} \geq 288.4615 \tag{8.27}$$

$$F_{3y} \leq 291.6667 \tag{8.28}$$

The torques in the previous equations are treated as absolute, since it could be either clock wise or counter clock wise. Widely used optimization algorithms for constrained optimization such as Genetic Algorithms and the Interior-Point Method could be used to minimize the maximum absolute torque amongst ($\tau_{11}, \tau_{12}, \tau_{21}, \tau_{22}, \tau_{31}$ and τ_{32}). However, such algorithms either take a long time to converge to a solution or highly dependent on the initial solution. In the next section, the problem is formulated to allow the use of linear programming algorithms.

7.2.4. Fitness Function Formulation

Although the problem could be solved using non-linear optimizers such as GA, nonetheless the problem could be reformulated to be efficiently solved using Linear programming. The reformulation could be accomplished as follows:

Let (8.21) to (8.26) be written in a matrix form as follows:

$$\mathrm{T} = A\mathcal{F} + \mathcal{B} \tag{8.29}$$

where T is a vector carrying the torques on the joints of the robot, A is the coefficient matrix $\mathcal{F}$ is the forces on the tips of the legs of the robot and $\mathcal{B}$ is a vector contains the constant coefficients of the torque equations.

In order to use linear programming, the problem of minimizing the maximum of absolute value equations was transformed into the linear programming standard form:

$$\min c^T y \tag{8.30}$$

$$s.t.\ \boldsymbol{A}y \geq \boldsymbol{b} \tag{8.31}$$

$$y \geq 0 \tag{8.32}$$

First, the nonlinear equations were transformed into linear, by removing the absolute sign from the equations and adding the same equations while changing the sign of the absolute terms, using Equation (8.15). Second, the max operator is removed by replacing (8.13) with one variable Y_f and the equations are rewritten in inequality equation format [70]. The function to be minimized is Y_f and the inequality equations are used as constraints. Finally, because linear programming works only with lower bounded variables, a lower bound on the variables was used. It was done by introducing another variable y_i, which is subtracted from every variable x_i. The terms of the linear programming form in (8.12), can be written as follows:

$$y^T = [Y_f \quad x_1 \quad x_2 \quad \dots \quad x_i \quad y_1 \quad y_2 \quad \dots \quad y_i] \tag{8.33}$$

where $i = 1,2, \dots, n$

$$c^T = [1 \quad 0 \quad 0 \quad \dots \quad 0] \tag{8.34}$$

$$\boldsymbol{A} = \begin{bmatrix} I_v & \mathcal{A} & -\mathcal{A} \\ I_v & -\mathcal{A} & \mathcal{A} \end{bmatrix} \tag{8.35}$$

$$\boldsymbol{b} = \begin{bmatrix} \mathcal{B} \\ -\mathcal{B} \end{bmatrix} \tag{8.36}$$

where c is a $(2m + 1)$ vector, with its elements are all zero except the first element. I_v is an $m \times 1$ vector, with its elements all ones. $\mathcal{B}$ is a vector contains the constant coefficients of $F_{ij}(x)$.

7.2.5. Solving with Different Algorithms

The problem is solved by using Genetic Algorithms, Pattern Search Algorithm, Nelder Mead Algorithm and a linear programming Algorithm, specifically, the Simplex algorithm. The stopping criteria for all of the algorithms except GA, were chosen to depend on the accuracy of the solution, while GA's stopping criteria was set to be based on time. The time was chosen to be the time required by the slowest of the other three algorithms to find a solution. Specifically, the maximum time for convergence was selected to be the time our algorithm took to find the exact solution of the problems considered. For Nelder Mead and Pattern Search algorithms, a random starting point is generated for every iteration of the 1000 tested runs.

The problem is solved using MATLAB on an Intel® Core® 2 Duo 2 GHz computer with 4GB DDR2 RAM. The precision of the software environment was up to 16 digits after the decimal point, which complies with the standards IEEE 754 for double precision used by MATLAB. To use the 16 digits accuracy, only the first 14 digits after the decimal point were used since the 16th digit had rounding error carried from the 17th digit. The term exact solution is used in the following text to refer to the solution associated to an error of 10^{-14}.

Table 7.1. The performance of the algorithms used to solve the problem

Comparison Property	Simplex Algorithm	Nelder-Mead Algorithm	Pattern Search Algorithm	Genetic Algorithm
Time (sec)	0.0125	0.053	0.2945	0.2945
Error (Best Solution)	0	2.27*10-13	0	128.4158
Error (Average Solutions)	0	130.027	27.3996	136.6092
Error (Worst Solutions)	0	5.09*103	89.9295	151.0992

The optimal solution for the problem is $F_{2x} = 166.6667$, $F_{3x} = 166.6667$, and $F_{3y} = 291.1992$. The optimal solution yields a maximum torque of 100. Table 7.1 shows the result of using the different algorithms to solve the robotics problem. It could be clearly seen that the fastest method to solve such a problem is the Simplex Algorithm, it was more than 4 times faster than the next fastest algorithm. The Simplex Algorithm's speed in finding the solution makes it suitable for real time applications.

The Simplex Algorithm also found the exact solution every run of the 1000 tested runs. The GA was not able to find an exact solution. If more time is given for the GA, it would produce a better solution. The worst solution is found by the Nelder-Mead algorithm because it highly dependent on the initial solution.

Chapter 8.

Conclusion and Future Work

This manuscript has investigated methods of optimizing the forces on climbing robots that use position controlled legs or force/torque controlled legs. This optimization is applicable for robots that use position controlled legs as well as force/torque controlled legs and seeks to minimize the maximum normal adhesion force on the tips of the legs. The maximum torque on the joints of the legs is also minimized for robots with force/torque controlled legs, while keeping the normal adhesion values on the tips of the legs of the robot at optimum levels.

Objective one, which is the minimization of the maximum normal adhesion force, is met by presenting a closed form solution, which computes the optimal normal adhesion force required on the tips of the legs of a climbing robot in order to adhere to vertical surfaces. The solution is found to depend on the position of the tips of the legs and the height of the robot, i.e. the distance between the center of mass and the climbing surface.

In order to meet objective two, the effect of a number of geometrical parameters on the maximum normal adhesion have been investigated independently. The robot was simplified into a two-dimensional structure with each leg simplified into a single straight beam. This simplification was validated by explaining the stance the ants use while they are loitering on vertical surfaces. It was found that ants position their middle legs' tip at approximately 0.61 to minimize the maximum normal adhesion force required to keep them on vertical surfaces. The effect of height, length, and the middle leg's position were investigated for both force/torque controlled robots and position controlled robots, while. the thickness of both the body and the legs and the inclination of the body and the legs were investigated for position controlled robots. The single-link legs were then replaced

with equivalent two-link legs. Calculating the normal adhesion force on the tips of the legs was done using FEM. Lastly, guidelines to design an optimal robotic structure that minimize the maximum normal adhesion are presented at the end of Chapter 5.

The problem of minimizing the maximum normal adhesion force of three-legged robots is a redundant problem with 2 DOF. Objective three uses this redundancy to minimize the maximum torque, for climbing robots with force/torque control legs, without affecting the optimal normal adhesion on the tips of the legs of the climbing robot. The optimization is carried out by transforming the non-linear problem into linear and solve the problem using the Simplex Algorithm. This method is found to be much faster, and more accurate compared to three widely used optimization algorithms.

The work presented in this manuscript opens up potential leads for further research:

- This work studies optimizing the forces on climbing robots considering the robots to be in a no motion state. Optimizing the forces while the robot is moving is an obvious extension to the presented work. This may include studying structures with four and five legs in order to design a suitable gait that minimizes the maximum adhesion force. It may also include designing a leg by choosing a proper links length, or joint placements, in order to optimize the torque on the joints.

- In Chapter 5, the inclinations angle of the legs are considered to be equal. An extension is to study the effect of using legs with different inclination angles.

- The two-links leg designs presented in Chapter 5 requires the use of an optimization algorithm to find an equivalent two-beams leg design to a single link leg. An extension is to find a closed form solution that computes the multi-beams design for any single-beam leg. Also, it would be interesting to see the effect of designing legs that have more than two-links.

- The analyzed robotic model considers each foot to be one single point on the climbing surface and considers no transfer of moment between the feet and the legs. An extension is to design the whole feet. The design could take into account the

height, the shape, and the stiffness of both the feet and the connection joint between the feet and the legs.

- The Simplex Algorithm used in Chapter 8 is tested on a dual core processor clocked at 2GHz with 4GB of memory. A challenging problem is to implement the optimization on microcontroller(s), such as Arduino Due, the fastest of the Arduino family, which has a single CPU clocked at 84MHz and a memory of 96KB, and allow it to run in real (or close to real) time.

In this thesis, the maximum normal adhesion force and the maximum torque are minimized. Minimizing the maximum normal adhesion force allows the use of weaker attachment mechanisms. That allows the climbing robots to both climb vertical surfaces with higher weight or payload, and increase the force that secures the robot on the climbed vertical surface. Minimizing the maximum torque allows using weak motors which reduces cost and weight.

References

[1] "Most Skyscrapers." [Online]. Available: http://www.emporis.com/statistics/most-skyscrapers.

[2] G. W. E. Council, "How many wind turbines are there in the world?" [Online]. Available: http://www.gwec.net/faqs/how-many-wind-turbines-world/.

[3] N. E. Institute, "World Statistics." [Online]. Available: http://www.nei.org/Knowledge-Center/Nuclear-Statistics/World-Statistics.

[4] Z. Xu and P. Ma, "A wall-climbing robot for labelling scale of oil tank's volume," *Robotica*, vol. 20, no. 02, pp. 209–212, Apr. 2002.

[5] W. Shen, J. Gu, and Y. Shen, "Permanent magnetic system design for the wall-climbing robot," *Appl. Bionics Biomech.*, no. July, pp. 2078–2083, 2006.

[6] J. Shang, B. Bridge, T. Sattar, S. Mondal, and A. Brenner, "Development of a climbing robot for inspection of long weld lines," *Ind. Robot An Int. J.*, vol. 35, no. 3, pp. 217–223, May 2008.

[7] N. Elkmann, T. Felsch, M. Sack, T. Böhme, J. Hortig, and J. Saenz, "Modular climbing robot for service-sector applications," *Ind. Robot An Int. J.*, vol. 26, no. 6, pp. 460–465, 1999.

[8] B. L. Luk, D. S. Cooke, S. Galt, A. A. Collie, and S. Chen, "Intelligent legged climbing service robot for remote maintenance applications in hazardous environments," *Rob. Auton. Syst.*, vol. 53, no. 2, pp. 142–152, Nov. 2005.

[9] H. X. Zhang, W. Wang, and J. W. Zhang, "High stiffness pneumatic actuating scheme and improved position control strategy realization of a pneumatic climbing robot," *2008 IEEE Int. Conf. Robot. Biomimetics*, pp. 1806–1811, Feb. 2009.

[10] W. Morris and J. Xiao, "City-climber: development of a novel wall-climbing robot," *J. Student Res. v1*, pp. 40–45, 2008.

[11] A. Parness, "Anchoring foot mechanisms for sampling and mobility in microgravity," *2011 IEEE Int. Conf. Robot. Autom.*, pp. 6596–6599, May 2011.

[12] L. R. Palmer III, E. D. Diller, and R. D. Quinn, "Design of a Wall-Climbing Hexapod for Advanced Maneuvers," in *International Conference on Intelignet Robots and Systems*, 2009.

[13] G. Haynes and A. Rizzi, "Gait Regulation and Feedback on a Robotic Climbing Hexapod," in *Proceedings of Robotics: Science and Systems*, 2006.

[14] A. T. Asbeck, M. R. Cutkosky, and W. R. Provancher, "SpinybotII: climbing hard walls with compliant microspines," in *ICAR '05. Proceedings., 12th International Conference on Advanced Robotics, 2005.*, 2005, pp. 601–606.

[15] B. Kennedy, A. Okon, H. Aghazarian, M. Badescu, X. Bao, Y. Bar-Cohen, Z. Chang, B. E. Dabiri, M. Garrett, L. Magnone, and S. Sherrit, “Lemur IIb: a robotic system for steep terrain access,” *Ind. Robot An Int. J.*, vol. 33, no. 4, pp. 265–269, 2006.

[16] H. Prahlad, R. Pelrine, S. Stanford, J. Marlow, and R. Kornbluh, “Electroadhesive robots—wall climbing robots enabled by a novel, robust, and electrically controllable adhesion technology,” in *2008 IEEE International Conference on Robotics and Automation*, 2008, pp. 3028–3033.

[17] G. Cui, K. Liang, J. Guo, H. Li, and D. Gu, “Design of a climbing robot based on electrically controllable adhesion technology,” *Proc. Int. …*, vol. 22, pp. 90–95, 2012.

[18] Y. Li, A. Ahmed, D. Sameoto, and C. Menon, “Abigaille II: toward the development of a spider-inspired climbing robot,” *Robotica*, vol. 30, no. 01, pp. 79–89, 2012.

[19] M. Henrey, A. Ahmed, P. Boscariol, L. Shannon, and C. Menon, “Abigaille-III: A Versatile, Bioinspired Hexapod for Scaling Smooth Vertical Surfaces,” *J. Bionic Eng.*

[20] A. Asbeck, S. Dastoor, A. Parness, L. Fullerton, N. Esparza, D. Soto, B. Heyneman, and M. Cutkosky, “Climbing rough vertical surfaces with hierarchical directional adhesion,” *2009 IEEE Int. Conf. Robot. Autom.*, pp. 2675–2680, May 2009.

[21] M. P. Murphy, C. Kute, Y. Menguc, and M. Sitti, “Waalbot II: Adhesion Recovery and Improved Performance of a Climbing Robot using Fibrillar Adhesives,” *Int. J. Rob. Res.*, vol. 30, no. 1, pp. 118–133, Oct. 2010.

[22] K. a. Daltorio, T. E. Wei, a. D. Horchler, L. Southard, G. D. Wile, R. D. Quinn, S. N. Gorb, and R. E. Ritzmann, “Mini-Whegs TM Climbs Steep Surfaces Using Insect-inspired Attachment Mechanisms,” *Int. J. Rob. Res.*, vol. 28, no. 2, pp. 285–302, Feb. 2009.

[23] J. Krahn, Y. Liu, a Sadeghi, and C. Menon, “A tailless timing belt climbing platform utilizing dry adhesives with mushroom caps,” *Smart Mater. Struct.*, vol. 20, no. 11, p. 115021, Nov. 2011.

[24] O. Unver and M. Sitti, “A miniature ceiling walking robot with flat tacky elastomeric footpads,” *2009 IEEE Int. Conf. Robot. Autom.*, pp. 2276–2281, May 2009.

[25] N. Wiltsie, M. Lanzetta, and K. Iagnemma, “A controllably adhesive climbing robot using magnetorheological fluid,” *2012 IEEE Int. Conf. Technol. Pract. Robot Appl.*, pp. 91–96, Apr. 2012.

[26] K. a. Daltorio, A. D. Horchler, S. Gorb, R. E. Ritzmann, and R. D. Quinn, “A small wall-walking robot with compliant, adhesive feet,” in *2005 IEEE/RSJ International Conference on Intelligent Robots and Systems*, 2005, pp. 3648 – 3653.

[27] M. Sitti, “Under-actuated tank-like climbing robot with various transitioning capabilities,” *2011 IEEE Int. Conf. Robot. Autom.*, pp. 777–782, May 2011.

[28] M. Osswald and F. Iida, “A climbing robot based on Hot Melt Adhesion,” in *2011 IEEE/RSJ International Conference on Intelligent Robots and Systems*, 2011, pp. 5107–5112.

[29] J. C. Grieco, M. Prieto, M. Armada, and P. G. De Santos, “A six legged climbing robot for high payloads,” in *Proceedings of the International Conference on Control and Applications, CCA*, 1998, no. September, pp. 446–450.

[30] S. Kim, S. Member, M. Spenko, S. Trujillo, B. Heyneman, D. Santos, and M. R. Cutkosky, “Smooth Vertical Surface Climbing With Directional Adhesion,” *IEEE Trans. Robot.*, vol. 24, no. 1, pp. 65–74, 2008.

[31] S. Kim and M. Spenko, “Whole body adhesion: hierarchical, directional and distributed control of adhesive forces for a climbing robot,” *Robot. …*, no. April, pp. 10–14, 2007.

[32] M. Cutkosky, “Stickybot III,” 2011. [Online]. Available: http://bdml.stanford.edu/twiki/bin/view/Rise/StickyBotIII.html.

[33] M. Spenko, G. Haynes, J. Saunders, M. Cutkosky, and A. Rizzi, “Biologically Inspired Climbing with a Hexapedal Robot,” *J. F. Robot.*, vol. 25, no. 4–5, pp. 223–242, 2008.

[34] B. B. L. Luk, A. Collie, V. Piefort, and G. Virk, “Robug III: A tele-operated climbing and walking robot,” in *UKACC International Conference on Control. Control ’96*, 1996, vol. 1996, no. 427, pp. 347–352.

[35] N. Xi, D. Aslam, H. Dulimarta, J. Xiao, and M. Minor, “Climbing the Walls,” no. December, pp. 10–19, 2002.

[36] K. D. Kotay and D. L. Rus, “Navigating 3D steel web structures with an inchworm robot,” in *Proceedings of IEEE/RSJ International Conference on Intelligent Robots and Systems. IROS ’96*, 1996, vol. 1, pp. 368–375.

[37] M. Abderrahim and C. Balaguer, “ROMA: a climbing robot for inspection operations,” *IEEE Robot. Autom.*, no. May, pp. 2303–2308, 1999.

[38] G. Wile and D. M. Aslam, “Design , Fabrication and Testing of a Miniature Wall Climbing Robot Using Smart Robotic Feet,” in *International Conference on Cybernetics and Information Technologies, Systems and Applications*, 2007, no. Servo 1, pp. 87–92.

[39] M. Tavakoli, a. Marjovi, L. Marques, and a. T. de Almeida, “3DCLIMBER: A climbing robot for inspection of 3D human made structures,” *2008 IEEE/RSJ Int. Conf. Intell. Robot. Syst.*, pp. 4130–4135, Sep. 2008.

[40] T. L. Lam and Y. Xu, “Treebot: Autonomous tree climbing by tactile sensing,” *2011 IEEE Int. Conf. Robot. Autom.*, pp. 789–794, May 2011.

[41] G. C. Haynes, a. Khripin, G. Lynch, J. Amory, a. Saunders, a. a. Rizzi, and D. E. Koditschek, “Rapid pole climbing with a quadrupedal robot,” *2009 IEEE Int. Conf. Robot. Autom.*, pp. 2767–2772, May 2009.

[42] J. Liu, Z. Tong, J. Fu, D. Wang, Q. Su, and J. Zou, “A gecko inspired fluid driven climbing robot,” *2011 IEEE Int. Conf. Robot. Autom.*, pp. 783–788, May 2011.

[43] R. A. S. De Los, G. M. Garduño, and L. A. González, “4Steel-Robot : A Climbing Mobile Robot for Gas Containers Inspection,” in *the 3rd WSEAS/IASME International Conference on Dynamical Systems and Control*, 2007, pp. 200–205.

[44] B. Kennedy, A. Okon, H. Aghazarian, M. Garrett, T. Hunts-, L. Magnone, M.

Robinson, and J. Townsend, “The Lemur II-Class Robots for Inspection and Maintenance of Orbital Structures : A System Description,” *Int. Conf. Climbing Walk. Robot.*, 2005.

[45] A. Sintov, T. Avramovich, and A. Shapiro, “Design and motion planning of an autonomous climbing robot with claws,” *Rob. Auton. Syst.*, vol. 59, no. 11, pp. 1008–1019, Nov. 2011.

[46] P. Birkmeyer, A. G. Gillies, and R. S. Fearing, “Dynamic climbing of near-vertical smooth surfaces,” *2012 IEEE/RSJ Int. Conf. Intell. Robot. Syst.*, pp. 286–292, Oct. 2012.

[47] Y. Yanagihara, T. Takubo, K. Ohara, Y. Mae, and T. Arai, “Optimization of grid wall walking by genetic algorithm,” *2009 Int. Conf. Mechatronics Autom.*, pp. 2665–2670, Aug. 2009.

[48] A. Saunders, D. I. Goldman, R. J. Full, and M. Buehler, “The RiSE Climbing Robot : Body and Leg Design,” in *Proc. SPIE Defence & Security Symposium, Unmanned Systems Technology*, 2006, no. April.

[49] O. Unver and M. Sitti, “Tankbot: A Palm-size, Tank-like Climbing Robot using Soft Elastomer Adhesive Treads,” *Int. J. Rob. Res.*, vol. 29, no. 14, pp. 1761–1777, Sep. 2010.

[50] R. Vidoni and A. Gasparetto, “Efficient force distribution and leg posture for a bio-inspired spider robot,” *Rob. Auton. Syst.*, vol. 59, no. 2, pp. 142–150, Feb. 2011.

[51] H. Russell, *Structural Analysis*, 8th ed. New Jersey: Pearson Education, 2012.

[52] M. E. H. Y. J. N. Z. Richard H. Byrd, “An interior point algorithm for large scale nonlinear programming.”

[53] R. A. Waltz, J. L. Morales, J. Nocedal, and D. Orban, “An interior algorithm for nonlinear optimization that combines line search and trust region steps,” *Math. Program.*, vol. 107, no. 3, pp. 391–408, Nov. 2005.

[54] C. Kyunghee, Y. Sungjae, J. Gihyun, and N. Kim, “Scheduling algorithm for real-time imprecise computations to minimise maximum weighted errors using the linear programming method,” *Electronics Letters*, vol. 33, no. 15. pp. 1301–1302, 1997.

[55] Z. Xiang, “Color image quantization by minimizing the maximum intercluster distance,” *ACM Trans. Graph.*, vol. 16, no. 3, pp. 260–276, Jul. 1997.

[56] W. Shufeng and Z. Yiren, “Scheduling to minimize the maximum lateness with multiple product classes in batch processing,” *TENCON ’02. Proceedings. 2002 IEEE Region 10 Conference on Computers, Communications, Control and Power Engineering*, vol. 3. pp. 1595–1598 vol.3, 2002.

[57] J. Mattingley and S. Boyd, “Real-Time Convex Optimization in Signal Processing,” *Signal Process. Mag. IEEE*, vol. 27, no. 3, pp. 50–61, May 2010.

[58] X. Lai, J. Wang, and Z. Xu, “A new minimax design of two-dimensional FIR filters with reduced group delay,” *Asian Control Conference, 2009. ASCC 2009. 7th*. pp. 610–614, 2009.

[59] G. Hornby and S. Takamura, “Autonomous evolution of dynamic gaits with two

quadruped robots," *Robot. , IEEE Trans.*, vol. 21, no. 3, pp. 402–410, 2005.

[60] B. Sheng, M. Huaqing, L. Qifeng, and Z. Xijing, "Multi-objective optimization for a humanoid robot climbing stairs based on Genetic Algorithms," *2009 Int. Conf. Inf. Autom.*, pp. 66–71, Jun. 2009.

[61] a. Kamimura, H. Kurokawa, E. Yoshida, S. Murata, K. Tomita, and S. Kokaji, "Automatic Locomotion Design and Experiments for a Modular Robotic System," *IEEE/ASME Trans. Mechatronics*, vol. 10, no. 3, pp. 314–325, Jun. 2005.

[62] M. Pang and Z. Chen, "Trajectory planning based on variable structure GA of a three-limbed robot," *2010 Int. Conf. Logist. Syst. Intell. Manag.*, pp. 611–614, Jan. 2010.

[63] K. Konolige, "A gradient method for realtime robot control," *Proceedings. 2000 IEEE/RSJ Int. Conf. Intell. Robot. Syst. (IROS 2000) (Cat. No.00CH37113)*, vol. 1, pp. 639–646, 2000.

[64] S. X. Yang and M. Q.-H. Meng, "A Knowledge Based Genetic Algorithm for Path Planning in Unstructured Mobile Robot Environments," *2004 IEEE Int. Conf. Robot. Biomimetics*, pp. 767–772, 2004.

[65] S.-D. Stan, V. Maties, and R. Balan, "Genetic algorithms multiobjective optimization of a 2 DOF micro parallel robot," *2007 IEEE Conf. Emerg. Technol. Fact. Autom. (EFTA 2007)*, pp. 780–783, Sep. 2007.

[66] N. Khurana, A. Rathi, and Akshatha P.S, "Genetic Algorithm: A Search of Complex Spaces," *Int. J. Comput. Appl.*, vol. 25, no. 7, pp. 13–17, 2011.

[67] M. Mitchell, "L.D. Davis, handbook of genetic algorithms," *Artif. Intell.*, vol. 100, no. 1–2, pp. 325–330, 1998.

[68] M. Gendreau and J.-Y. Potvin, Eds., *Handbook of Metaheuristics*, Second. New York: Springer, 2010.

[69] N. Durand and J. Alliot, "A Combined Nelder-Mead Simplex and Genetic Algorithm," in *GECCO-99: Proc. Genetic and Evol. Comp. Conf*, 1999, pp. 1–7.

[70] G. B. Dantzig and M. N. Thapa, *Linear Programming 1: Introduction*. Secaucus, NJ, USA: Springer, 1997.

[71] D. Z. Chen, Y. Gu, J. Li, and H. Wang, "Algorithms on Minimizing the Maximum Sensor Movement for Barrier Coverage of a Linear Domain," p. 28, Jul. 2012.

[72] G. McKnight and C. Henry, "Variable stiffness materials for reconfigurable surface applications," in *Smart Structures and Materials*, 2005, pp. 119–126.

[73] C. L. DAVIS and G. A. LESIEUTRE, "An Actively Tuned Solid-State Vibration Absorber Using Capacitive Shunting of Piezoelectric Stifness," *J. Sound Vib.*, vol. 232, no. 3, pp. 601–617, May 2000.

[74] K. . Otsuka and C. M. Wayman, *Shape Memory Materials*, First. Cambridge University Press, 1999.

[75] Z. G. Wei, R. Sandstrom, and S. Miyazaki, "Shape memory materials and hybrid composites for smart systems: Part I Shape-memory materials," *J. Mater. Sci.*, vol. 33, no. 15, pp. 3743–3762, 1998.

[76] A. Lendlein and S. Kelch, “Shape-Memory Polymers,” *Angew. Chemie Int. Ed.*, vol. 41, no. 12, p. 2034, Jun. 2002.

[77] F. Gandhi and S.-G. Kang, “Beams with controllable flexural stiffness,” *Proc. SPIE*, vol. 6525. p. 65251I–65251I–8, 2007.

[78] H. Moein and C. Menon, “Smart compression bandage using shape memory alloy artificial muscle as a potential remedy for lower extremity disorders,” in *8th World Congress on Biomimetics*, 2015.

[79] I. Pretto, Y. Li, S. Cocuzza, S. Deb, and C. Menon, “Contact Forces Optimization of a Bio-Inspired Climbing Robot,” *CAES 2011 Int. Conf. Eur. Aerosp. Socities*, 2011.

[80] A. Ahmed and C. Menon, “Adhesion Optimization of Climbing Robotic Structure through Changing the Legs’ Elasticity,” in *The 5th International Conference on Smart Materials and Nanotechnology in Engineering*, 2015.

[81] E. W. Hawkes, J. Ulmen, N. Esparza, and M. R. Cutkosky, “Scaling walls: Applying dry adhesives to the real world,” *IEEE Int. Conf. Intell. Robot. Syst.*, pp. 5100–5106, 2011.

[82] M. P. Murphy, S. Member, and M. Sitti, “Waalbot : An Agile Small-Scale Wall-Climbing Robot Utilizing Dry Elastomer Adhesives,” in *IEEE/ASME Transactions on mechatronics*, 2007, vol. 12, no. 3, pp. 330–338.

[83] P. Boscariol, M. A. Henrey, Y. Li, and C. Menon, “Optimal Gait for Bioinspired Climbing Robots Using Dry Adhesion: A Quasi-Static Investigation,” *J. Bionic Eng.*, vol. 10, no. 1, pp. 1–11, Jan. 2013.

[84] A. Gasparetto, R. Vidoni, and T. Seidl, “Kinematic study of the spider system in a biomimetic perspective,” *2008 IEEE/RSJ Int. Conf. Intell. Robot. Syst.*, pp. 3077–3082, Sep. 2008.

[85] S. S. Rao, *Mechanical Vibrations*, 2nd ed. Addison-Wesley, 1990.

[86] A. Ahmed and C. Menon, “On the Static Structural Design of Climbing Robots: Part 1,” *J. Robot. Biomimetics*, vol. Submitted, 2015.

[87] A. Ahmed and C. Menon, “On the Static Structural Design of Climbing Robots: Part 2,” *J. Robot. Biomimetics*, 2015.

[88] D. Santos, B. Heyneman, S. Kim, N. Esparza, and M. R. Cutkosky, “Gecko-inspired climbing behaviors on vertical and overhanging surfaces,” *2008 IEEE Int. Conf. Robot. Autom.*, pp. 1125–1131, May 2008.

[89] A. Ahmed and C. Menon, “Optimizing the Maximum Torque of bioinspired climbing robots in static equilibrium,” in *IEEE RAS/EMBS International Conference on Biomedical Robotics and Biomechatronics*, 2016.

[90] J. J. Craig, *Introduction to Robotics, Mechanics and Control*, Third Edit. Pearson Education, 2005.

[91] M. W. Jeter, *Mathematical Programming*. New York, 1986.

Appendix A.

Stiffness of the materials does not affect the force distribution (Proof)

In this Appendix we show that the use of different materials does not change the results of the geometrical optimization that is performed. In fact, the stiffness matrix for one beam is given by:

$$\boldsymbol{F} = \begin{bmatrix} \frac{AE}{L} & 0 & 0 & -\frac{AE}{L} & 0 & 0 \\ 0 & \frac{12EI}{L^3} & \frac{6EI}{L^2} & 0 & -\frac{12EI}{L^3} & \frac{6EI}{L^2} \\ 0 & \frac{6EI}{L^2} & \frac{4EI}{L} & 0 & -\frac{6EI}{L^2} & \frac{2EI}{L} \\ -\frac{AE}{L} & 0 & 0 & \frac{AE}{L} & 0 & 0 \\ 0 & -\frac{12EI}{L^3} & -\frac{6EI}{L^2} & 0 & \frac{12EI}{L^3} & -\frac{6EI}{L^2} \\ 0 & \frac{6EI}{L^2} & \frac{2EI}{L} & 0 & -\frac{6EI}{L^2} & \frac{4EI}{L} \end{bmatrix} \cdot \boldsymbol{D} \tag{A1}$$

where E is the elasticity coefficient, A is the cross sectional area of the beam, L is the length of the beam and I is the inertia of the beam. Assuming all of the cross sections of the beams is a circle; the second moment of inertia for a circular cross section is:

$$I = \frac{\pi r^4}{4} = \frac{Ar^2}{4} \tag{A2}$$

Factoring out E, A and L can be written as:

$$F = \frac{A \cdot E}{L} \begin{bmatrix} 1 & 0 & 0 & -1 & 0 & 0 \\ 0 & \frac{3r^2}{L^2} & \frac{3r^2}{2L} & 0 & -\frac{3r^2}{L^2} & \frac{3r^2}{2L} \\ 0 & \frac{3r^2}{2L} & r^2 & 0 & -\frac{3r^2}{2L} & \frac{r^2}{2} \\ -1 & 0 & 0 & 1 & 0 & 0 \\ 0 & -\frac{3r^2}{L^2} & -\frac{3r^2}{2L} & 0 & \frac{3r^2}{L^2} & -\frac{3r^2}{2L} \\ 0 & \frac{3r^2}{2L} & \frac{r^2}{2} & 0 & -\frac{3r^2}{2L} & r^2 \end{bmatrix} \cdot D \tag{A3}$$

$$F = \left[\frac{A \cdot E}{L} \cdot K_E\right] \cdot D \tag{A4}$$

$\boldsymbol{K_E}$ is the stiffness matrix multiplied by $\frac{L}{\boldsymbol{A \cdot E}}$. In the same way, $\frac{\boldsymbol{A \cdot E}}{L}$ can be taken as a common factor from all of the elements of the stiffness matrix in Equation (4.6), which can be rewritten as:

$$\boldsymbol{F_u} = \left[\frac{A \cdot E}{L} \cdot \boldsymbol{K_{E21}}\right] \cdot \left[\frac{A \cdot E}{L} \cdot \boldsymbol{K_{E11}}\right]^{\boldsymbol{-1}} \cdot \boldsymbol{F_k} \tag{A5}$$

$$\boldsymbol{F_u} = \frac{A \cdot E}{L} \cdot \boldsymbol{K_{E21}} \cdot \frac{L}{A \cdot E} \cdot \boldsymbol{K_{E11}^{-1}} \cdot \boldsymbol{F_k} \tag{A6}$$

The above equation can be written as:

$$\boldsymbol{F_u} = \boldsymbol{K_{E21}} \cdot \boldsymbol{K_{E11}^{-1}} \cdot \boldsymbol{F_k} \tag{A7}$$

It can be seen that Equation (A7) is independent of the elasticity coefficient E. In other words, the elasticity of the beams relative to each other is what causes the change in the force distribution.

Appendix B

Normal and Shear Force Distribution

Shear force distribution due to middle leg's position

A structure with a height to body length aspect ratio of 1:2 is arbitrarily selected to explain the behavior of the normal force distribution due to changing the middle leg's position. The shear force distribution on the legs of a robot with body length of 200, and height of 100 is shown in Figure B.1. The behavior of the force distribution for a three-legged robot is similar for different height to length ratios. The shear force distribution for the middle leg always has a peak at middle leg's position of 0.5, while the front leg has a maximum at middle leg's position of 0, and the hind leg has a maximum at middle leg's position of 1. The normal force, in Figure 5.1, for the middle leg has a minimum and a maximum at middle leg's position value close to 0 and 1 respectively, the front leg has one peak close to middle leg's position of 1 and the hind leg has one negative peak at a middle legs position of 0.

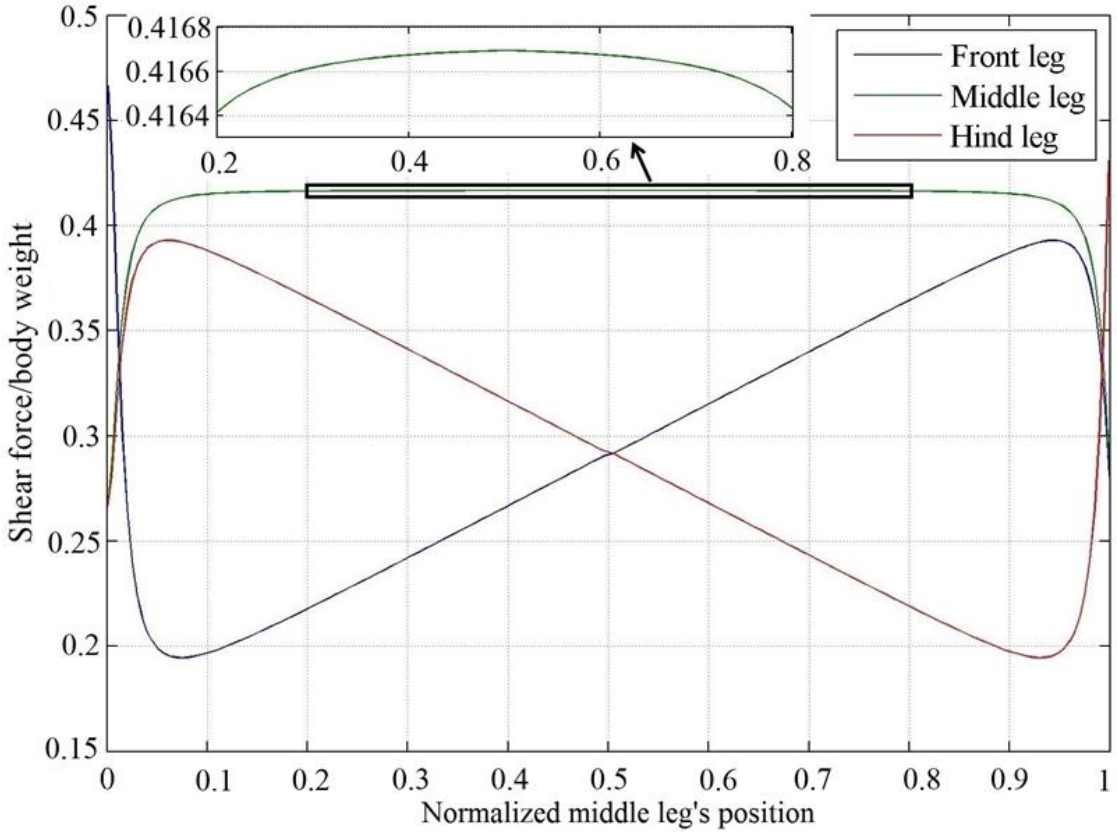

Figure B.1. Shear force distributions on the tips of the three legs for different positions of the middle leg.

A rationale to understand the behavior shown in Figure B.1 is hereafter presented. Let us consider a robot on a vertical surface (See Figure B.2-a). Due to the effect of its weight, the legs deflect backward and act as springs with equal spring constants. Therefore, the cg, the hip joints of the front leg (J_{Hf}), the middle leg (J_{Hm}) and front leg (J_{Hh}) are displaced backward by a distance $\delta_{cg}, \delta_f, \delta_m$ and δ_h respectively (see Figure B.2-b). The induced shear forces on the tips of the legs are directly proportional to the displacements $\delta_h, \delta_{\mathrm{m}}$ and δ_f, because the legs are assumed to be identical to each other.

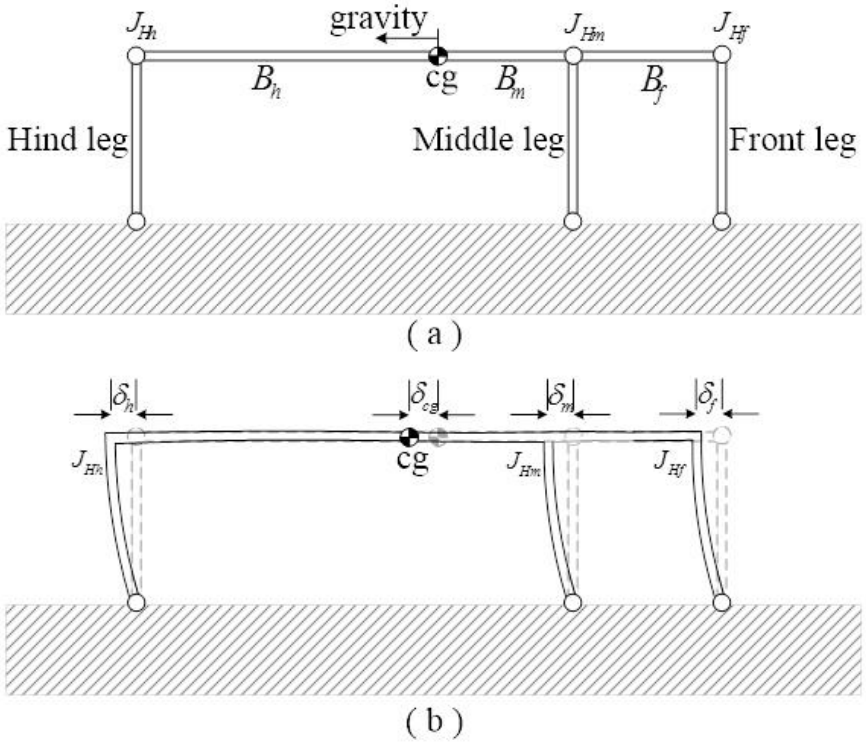

Figure B.2. The deflection in the robot's structure due to its weight when loitering on a vertical surface (a) the un-deflected structure, and (b) the deflected structure.

Figure B.2, which is obtained through an ANSYS simulation, shows the deflections in the structure. In Figure B.2, B_m is the beam connecting J_{Hm} to cg. B_f and B_h are instead the beams connecting J_{Hf} to J_{Hm} and J_{Hh} to cg respectively when the middle leg is located between cg and J_{Hf}. These two parameters, that is B_f and B_h, are the beams connecting J_{Hf} to cg and J_{Hh} to J_{Hm} respectively when the middle leg is located between cg and J_{Hh}.

When the middle leg is located between the center of mass and the front leg, the body's deflection creates a compression in B_m and B_f and an expansion in B_h thus causing the distances δ_f, δ_m and δ_h to be less than δ_{cg}. The distance δ_h is equal to the compression in B_h subtracted from δ_{cg}; also, δ_m is equal to the elongation in B_m subtracted from δ_{cg}, and δ_f is equal to the compression in B_f subtracted from δ_m.

The maximum distance that J_{Hm} travels is when it is located at the center of mass cg, which corresponds to the maximum force it experiences. The expansion in B_f and the compression in B_h cause δ_f and δ_h to be less than δ_m; these expansion and compression generate less shear force in the hind and the front legs than that in the middle one (see Figure B.1when the middle leg's position is at 0.5). The front and middle legs have the same shear force when the middle leg's position is at 1, because, δ_m and δ_f are equal. The amount of expansion in B_f increases with the length, causing δ_f to be smaller than δ_m and thus generating less shear force in the front leg than that in the middle one (see Figure B.1 for a middle leg's position ranging between 0.5 and 1).

The case when the middle leg is located between the center of mass and the hind leg could be analyzed as done previously. The main difference is that the beam B_m undergoes compression instead of expansion.

Normal-force distribution due to middle leg's position

The normal force distribution at different middle leg's positions is shown in Figure B.3. The distribution of the force on the tips of the legs can be explained by dividing the robot into two sub-structures at J_{Hm}. The first sub-structure, when the middle leg's position is located between 0.5 and 1, is composed of the middle leg, B_f and the front leg while the second sub-structure is composed of B_m, B_h and the hind leg. The first sub-structure, when the middle leg is positioned between 0 and 0.5, is composed of the middle leg, B_h and the hind leg and the second sub-structure is composed of B_m, B_f and the front leg.

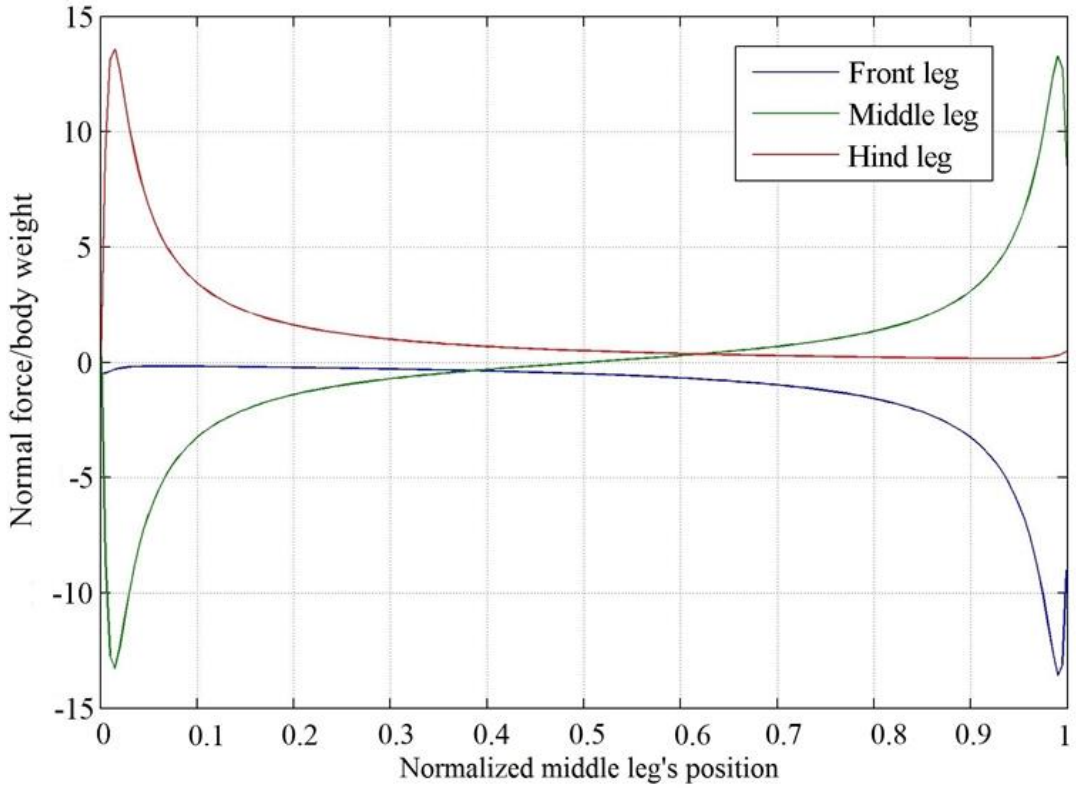

Figure B.3. Normal force distribution on the tips of the legs for different middle leg's positions. The maximum adhesion force follows the profile of the green line in the 0-0.38 range and the blue line in the 0.38-1 range.

The second sub-structure, formed by the hind leg, B_h and B_m, when the middle leg's position between 0.5 and 1, applies a wrench to the first sub-structure, formed by the middle and the front legs with B_f; the wrench is comprised of F_L which has the same direction as the gravitational force towards the negative x-axis, a shear F_P towards the positive y-axis, and a torque τ applied at J_{Hm}. The effect of the wrench can be analyzed by considering the structure that contains the middle leg, the front leg and B_f in Figure B.4. The effect of the individual components of the wrench is explained as follows:

First, the effect of τ_L: applying a torque τ_L at J_{Hm} causes a tension force to be generated in the front leg and a compression force in the middle leg. A decrease in the length of B_f, due to a change in the middle leg's position towards the front, causes an increase in the tension and the compression magnitude in the front and middle legs, and vice versa.

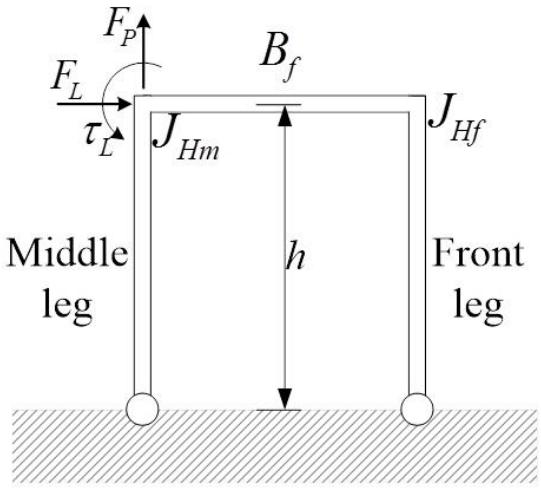

Figure B.4. Structure of a 2-legged robot

Second, the effect of F_L: applying force F_L at J_{Hm} causes a tension force to be generated in the middle leg and a compression force in the front leg. A decrease in the length of B_f , due to a change in the middle leg's position, causes an increase in the amount of the tension and compression, and vice versa. Third, the effect of F_P: applying force F_P in the positive direction of the y-axis at J_{Hm} causes a tension force in only the middle leg, i.e. a decrease in the normal force of the middle leg.

Each of the first two wrench components, namely τ_L and F_L, cause opposite forces along the middle and the front legs, thus causing the big difference in the normal forces of the middle and front legs, which are colored green and blue in Figure B.3. The difference in the forces is a result of the opposite forces generated in the middle and front legs by τ_L and F_L.

The case when the middle leg is positioned between 0 and 0.5 can be analyzed similarly. The second sub-structure, formed by B_m, B_f and the front leg, applies a wrench to the first sub-structure, formed by the middle leg, B_h and the hind leg, at J_{Hm} while the normal force at the tips is a result of the wrench applied. The deflected shapes for different configurations of the robot are shown in Figure B.5.

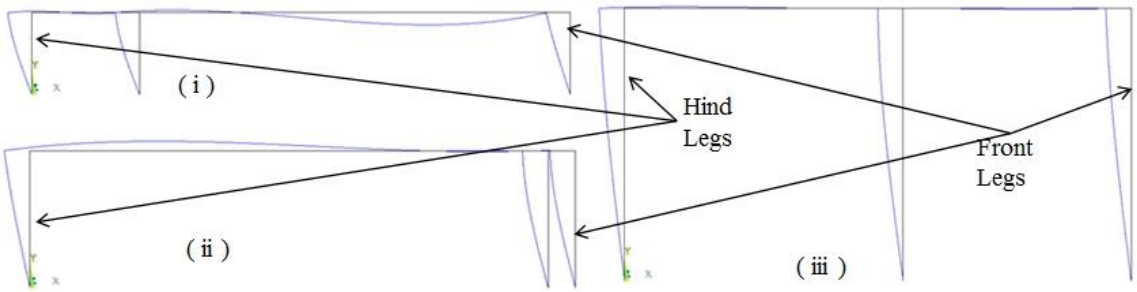

Figure B.5. **This figure shows the deflection of the structure of a robot for different heights and middle leg's positions. The body has body length of 200, elasticity of 1.12×10^9 and a unit weight. (i) The height is 30 and d_r is equal to 40. Note that the deflection is magnified by 1.95×10^5 times. (ii) The height is 50 and d_r is equal to 190. Note that the deflection is magnified by 626.7 times. (iii) The height is 100 and d_r is equal to 110. The deflection is magnified by 8928.4 times.**